DIPLOMA THESIS

Glucose transport and inhibition in five human organ barriers

Submitted at the Faculty of Analytical Chemistry,
Vienna University of Technology
in partial fulfilment of the requirements for the degree of
Diplom-Ingenieur (equals Master of Sciences)

under supervision of

Univ.Prof. Dipl.-Ing. Dr. Peter Ertl
Projetass. Dr.nat.techn. Mario Rothbauer

Institute of Applied Synthetic Chemistry (E163)

Vienna University of Technology

by

Jasmin Pajenda
Matr. Nr. 01125629
Theresiengasse 40/6, 1180 Wien

3.10.2018 _____

Erklärung

Hiermit erkläre ich, dass die vorliegende Arbeit ohne unzulässige Hilfe Dritter und ohne Benutzung anderer als der angegebenen Hilfsmittel angefertigt wurde. Die aus anderen Quellen oder indirekt übernommenen Daten und Konzepte sind unter Angabe der Quelle gekennzeichnet.

Die Arbeit wurde bisher weder im In- noch im Ausland in gleicher oder in ähnlicher Form in anderen Prüfungsverfahren vorgelegt.

Wien, am 3.10.2018 _____

Jasmin Pajenda

Abstract

The current work handles the comparative characterisation of five distinct organ barriers in regard to transport and inhibition of glucose. The organs of the lung, placenta, liver and intestines were represented by cancer cell lines in in-vitro barriers models. As the transport of glucose is controlled by various active and passive glucose transporters, different inhibitors of the passive facilitate glucose transporter (GLUT) family and/or the active sodium-glucose linked transporter (SGLT) family were tested. Prior, the barrier integrity was assessed with the transepithelial/endothelial resistance and sodium fluorescein leakage assays.

Cytochalasin B (CB) reduced sugar transport by 52% in the placental BeWo b30 and by 42% in the hepatic Hep G2 barrier due to inhibition of the highly expressed passive transporters GLUT1 and GLUT3. A moderate inhibition of 34% of GLUT1, 3 4 and 12 in the lung A549 barrier with CB was identified. The intestinal barriers Caco-2 and HT-29 showed an overall low inhibition of 19% with CB as GLUT2 and SGLT1 transporters were not inhibited and presumably responsible for the majority of glucose transport apart from GLUT1. In contrast, phloretin (PT) binds to the receptors of GLUT2 and SGLT1 and achieved a reduction of up to 45% in the intestinal cancer barriers. However, due to its lower inhibitory strength in GLUT1 and GLUT4, overall lower inhibition rates of 20% in lung, 38% in placental and 36% in hepatic barriers were accomplished. The results suggest that in placental and hepatic barriers the glucose transfer is mainly contributed to GLUT1 and GLUT3, and the glucose transport in intestinal barriers to GLUT2 and SGLT1.

Danksagung

An erster Stelle möchte ich mich bei meinen Eltern Jamila und Gholam Sachi Pajenda bedanken. Sie haben mich ermutigt ein universitäres Studium zu beginnen und mich auf dem Weg zum Abschluss stets begleitet und unterstützt. Ich möchte mich bedanken, dass sie mir ein sorgenfreies Studium ermöglicht haben.

Ich möchte mich bei Peter Ertl für seine Betreuung herzlich bedanken. Seine fachlichen Anregungen gemeinsam mit vielen konstruktiven Diskussionen waren eine große Hilfe für diese Arbeit.

Für die intensive Betreuung von Mario Rothbauer möchte ich mich bedanken. Seine fachliche Unterstützung und produktiven Anregungen haben mir bei dieser Arbeit sehr geholfen.

Contents

Abbreviations

ATP	Adenosine triphosphate
AB	Antibiotics
ATR	Attenuated total reflection
BBB	Blood-brain barrier
CA AM	Calcein AM
$CaCl_2$	Calcium chloride
CO_2	Carbon dioxide
CB	Cytochalasin B
DMEM	Dulbecco's Modified Eagle Medium
PBS	Dulbecco’s Phosphate Buffered Saline
Em	Emission
Ex	Excitation
EthD-1	Ethidium Homodimer-1
FBS	Fetal bovine serum
FT	Fourier-transform
FTIR	Fourier-transform infrared
GLUT	Glucose transporter
HMIT	H+/myo-inositol symporter
IR	Infrared
IUGR	Intrauterine growth restriction
LOD	Limit of detection
LOQ	Limit of quantification
$MgCl_2$	Magnesium chloride
MIR	Mid infra-red
MEM	Modified Eagle's medium
NEAA	Non-essential amino acids
OXPHOS	Oxidative phosphorylation
PT	Phloretin
PZ	Phlorizin

PB	PrestoBlue™
RPMI	Roswell Park Memorial Institute
RMS	Root mean square
SGLT	Sodium-glucose linked transporter
Na-flu	Sodium fluorescein leakage
TEER	Transepithelial/endothelial resistance

1. Introduction

1.1. Importance of glucose in the human body

Glucose supplies energy to every cell in the human body and performs vital metabolic functions to sustain life. The sugar is transported in the body either through paracellular transport paths or with special transport membrane proteins. They include facilitate glucose transporters (GLUTs) in the direction of the electrochemical gradient of glucose, or active sodium-glucose linked transporter (SGLTs) against the gradient [1, 2]. The fundamental mechanisms and transport ways of glucose are handled in more detail in Section 1.2.1 Pathways of transport.

Glucose from ingested food is mainly absorbed in the intestines and afterwards distributed to the rest of the body to provide energy. The intestinal transport way of glucose is directed in one direction from the lumen of the intestine through the intestinal barrier into the intestinal bloodstream. In addition to paracelluar transport pathways, transport of glucose in the intestines is enabled with the corporation of active and passive glucose transporters. Problems in the transport through the intestinal barrier can cause severe dehydration and diarrhoea. A mutation in the gene of SGLT1, the primary active transporter in the intestines, can lead to malabsorption of glucose and galactose. It mostly affects the transport of glucose in the intestine and usually ends fatal [3, 4].

The liver regulates the glucose levels in the blood. In the liver glucose from the intestinal bloodstream is stored as glycogen and released when necessary. A particular important glucose transporter is GLUT2, which handles the release of glucose from the liver into the blood. Defects in the gene of GLUT2 can result in an accumulation of glycogen in the liver, named Fanconi-Bickel syndrome [5, 6].

The by far highest glucose consumption exhibits the human brain. The transport pathways of glucose are accomplished by passive glucose transporters through the blood-brain barrier (BBB). The high requirement of glucose offer many targets for various disorders of the brain in case of glucose deficiency. Constantly low sugar supply can cause neuroglycopenia, a neurodevelopmental deficiency syndrome. The syndrome can interrupt brain development and is accompanied by atypical movements, muscle tones and retardation. Also, a mutation in the gene of GLUT1 is the initial cause for GLUT1-deficiency syndrome and damages the glucose transport through the blood-brain barrier [7, 8].

Another crucial transport of glucose is accomplished by the placenta, an organ that develops during pregnancy. The placenta is the most important coupling between mother and fetus. Its main function is the delivery of oxygen, glucose and other nutrients to the fetus. The glucose transporters in the placenta control the sugar transfer to the fetus [9]. Complication in glucose regulation can cause serious complications during pregnancy. Defects in placental transport can restrict the delivery of necessary nutrients to the fetus and can lead to physical deficiencies, known as intrauterine growth restriction (IUGR) [10]. Contrary to IUGR, other abnormalities in the fetal nutrition can be observed in the case of maternal diabetes. Here, an overgrowth in the child is observable due to the excess and overflow of nurturing glucose to the child. It leads to hyperinsulinemia and encourages fat accumulation in the fetus [11].

Contrary to other organs, the lung does not have a specific task in regard to glucose metabolism. However, the particular distribution of glucose transporters in the lung are suggested to be part of a defence mechanism. The proposal arises from the strong expression of high affinity glucose transporter at the air-lung side, and low affinity glucose transporters at the lung-blood interface. The configuration is beneficial to maintain low glucose concentrations in the lung and prevent the distribution of infections [12].

Glucose transporters are important for the investigation of diseases and basis of research and treatment options. In order to conduct research, it is essential to develop techniques that enable the investigation of glucose transport or drugs across these human organ barriers.

In-vitro studies give the possibilities to study the activity of glucose transporters with the advantage of the absence of animal testing [13]. In models of organ barriers, cells of the according organ are used to create barriers with physiological properties of the organs [14]. Therefore, the current thesis focuses on barrier models of various organs and their transport properties in respect to glucose transporter in in-vitro models.

1.2. Transport, inhibition and detection of glucose

The transport of glucose in the body plays a critical role in the metabolism and supply, since it is the most important source of energy for cells. Therefore, the understanding of the underlying principles of transport pathways is essential and explained first before discussing glucose transport mechanisms. Later, various glucose transporters found in the body and their tissue distributions are handled and summarized in more detail. Afterwards, differences in occurrences of glucose transporter between healthy and cancerous cells are described. Finally, different inhibition mechanisms of glucose transporters, and the detection of glucose with infrared absorbance spectroscopy among others, are discussed.

1.2.1. Pathways of transport

The first transport model discussed, describes if a solute is carried through the cell or has its transport route through the intercellular space between cells. In the transcellular transport the pathway of a substance crosses the cell and cell membrane. In contrast, the paracellular path of a substance is through, with or without modulators of tight junctions, between cells. Both pathways are sketched in

Figure 1.1.

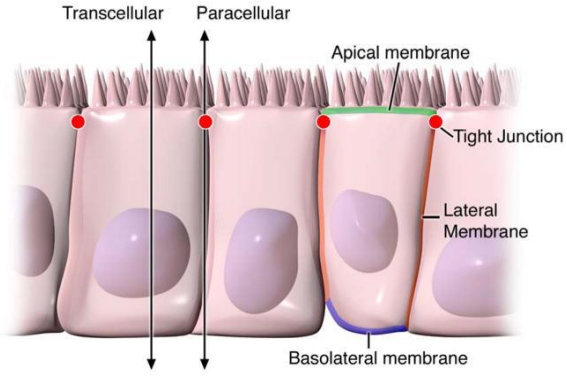

Figure 1.1: Transcellular and paracelluar transport models. Transport through the cell is called transcellular, transport between the cells is referred to as paracellular transport. Picture derived from [15].

The paracellular path is physiologically important in regard to the transport of ions, glucose, amino acids, and others for concentrations exceeding the amount of carrier transporters. The level of importance is dependent on the type of tissue, e.g. the small intestine allows more paracellular passage than the colon as its main function is to absorb the nutrients [2].

The transcellular transport of solutes through a cell can be described based on several criteria: the direction of the transport, energy consumption and transport type through the cell membrane of a single cell. In case of energy consumption, a distinction can be made between the active and passive transport across cell membranes for transcellular transport. The main difference between active and passive transport is, whether metabolic energy (active) or the kinetic energy of a concentration gradient (passive) is required for the transport [2].

The passive transport can be further split into three categories: (1) simple diffusion, (2) osmosis and (3) facilitated diffusion. In simple diffusion very small and non-polar particles move along the concentration gradient from a higher to a lower concentration. Osmosis is the particular diffusion of water molecules through a cell membrane. In facilitated diffusion larger or charged molecules are transported with membrane transport channels along the concentration gradient. Facilitated diffusion does not require cellular energy for the transport, because they transport from a higher concentration gradient to a lower and not against it, as it is the case for active transport. This type of transport is specific for certain types of molecules and is the underlying principle of the GLUT transporter family [16]. The GLUT family is discussed in more detail in Section 1.2.2 Glucose transport and families.

The active transport is able to transfer molecules against the electrochemical gradient of the transport molecule. It distinguishes between: (1) primary (direct) and (2) secondary (indirect) active transport. It is called primary or secondary active transport based on if ATP is directly coupled in the process or if the transport depends on a concentration gradient. The secondary active transport works carrier mediated. It couples the molecule of interest, e.g. glucose, indirectly with a carrier molecule and moves it along the concentration gradient of the carrier molecule, but against the gradient of the molecule of interest [16-19]. This enables the transport of a molecule against their concentration gradient. The process works without the direct usage of ATP. Instead it uses the gradient of the carrier molecule created by primary active transport [20].

1.2.2. Glucose transport and families

In general, the transport mechanism of a substance is specific, it depends on what is being transported. Glucose is a simple hexose sugar molecule with a ring shaped structure and consists of six carbon (C), twelve hydrogen (H) and six oxygen (O) atoms, its structure can be seen in Figure 1.2 [3, 21].

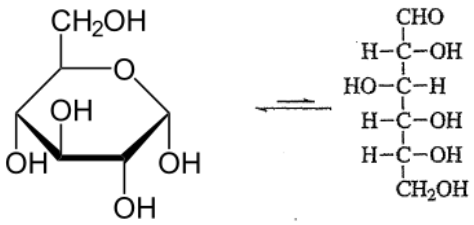

Figure 1.2: Structures of D-glucose ($C_6H_{12}O_6$); right shows the Fisher projection of D-glucose and left the Haworth projection of α-D-glucose. Pictures derived from [22, 23].

Glucose is a polar molecule and too large to be transported by simple diffusion. However, there exist three transport ways for glucose: through paracellular transport, facilitated diffusion or active transport. The type of glucose transport in turn depends on the function and needs of the specific tissue and cells. A vivid example is the intestinal tissue, where glucose should only be transported in one direction, namely from the gut to the intestinal blood stream, regardless of the concentration gradient [2, 24].

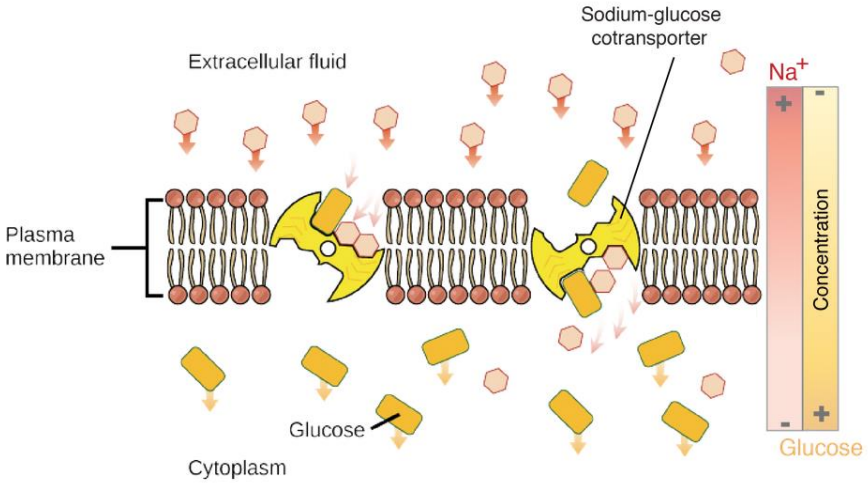

Figure 1.3: In secondary active transport the molecule of interest is transported against its concentration gradient and along the concentration gradient of the co-transporter. The image shows the principle of the sodium-dependent glucose transport. Picture derived from [19].

In these type of tissues a high expression of primary active glucose transporters can be found. In addition, the heart, the brain and the kidney are also known to participate in secondary active transport processes of glucose. For instance, in these organs the sodium-dependent glucose transport protein 1 (SGLT1) co-transports sodium together with glucose in a ratio of 2:1. Figure 1.3 illustrates the transport of glucose against its concentration gradient with the help of a sodium glucose co-transporter [20, 25].

On the other hand, facilitated diffusion processes are used to regulate or generate even glucose concentrations among tissues. The facilitated transport is shown in Figure 1.4, where the glucose is transported along its concentration gradient with the help of a glucose carrier.

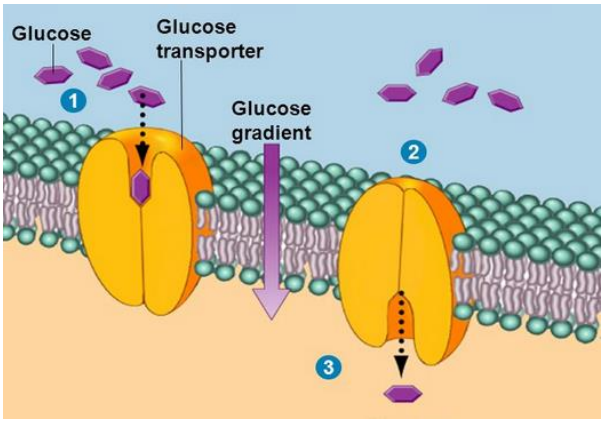

Figure 1.4: The passive facilitated transport of glucose through the plasma membrane with the help of glucose carriers is shown. Glucose is transported along its concentration gradient. Picture is derived from [26].

The transport of glucose is handled by two families of transport proteins. The two transporter families are differentiated based on the type of the transport mechanism. The glucose transporter family GLUT is performing passive facilitated diffusion and the sodium-glucose linked co-transporter family SGLT is following secondary active transport mechanisms [27, 28].

1.2.2.1. The GLUT transport family

The facilitated GLUT transporter family has 14 members of which all except GLUT13/HMIT (H+/myo-inositol symporter) are facilitate transporters [29]. A complete list of all GLUT family members regarding their functions, tissue distributions and known linked diseases is provided in

Table 1.1. The GLUT members are assigned into three classes based on the similarity of their gene sequences: class I includes GLUT1-4 and 14, class II contains GLUT5, 7, 9 and 11, class III is comprised of the remaining GLUT6, 8, 10, 12 and 13/HMIT. Of all classes, GLUTs of class I and GLUT5 of class II are the most studied transporters and manifest their roles as glucose (GLUT1-4) and fructose (GLUT2, 5) transporters [30].

Not every facilitate transporter has the same affinity to glucose. The lowest affinity of the GLUT family exhibits GLUT2 with a Michaelis constant, Km, of 17mM for glucose. The GLUT member with the highest affinity and lowest Km constant is GLUT10 with 0.3 mM [31]. The facilitate GLUT1 transporter shows a Km of 3.4 mM for glucose in rats [32]. It is most common subtype of the family and present in a broad variety in many fetal tissues, placental tissue, and is also an important

transporter in the epithelial blood-brain and blood-tissue barriers [27]. In the placenta, GLUT1 is significantly expressed in the microvillus and basal membranes, but has a higher occurrence in the microvillus site than in the basal site. It is highly involved in the transfer of glucose through the placenta. The lower concentration of GLUT1 on the basal side primary defines the glucose release [33].

The subtype GLUT3 has a higher affinity for glucose than GLUT1 and is expressed in tissues where glucose is crucial for the metabolism. It was also shown that GLUT3 is present in the microvillus membrane of the placenta in the first trimester of pregnancy. However, the presence of GLUT3 decreases as the pregnancy progresses, indicating that it is important in the early phase of pregnancy to ensure sufficient glucose supply to the fetus [34]. The transporter GLUT3 is also linked to fulfil the main transport through the blood-brain barrier. The high affinity of GLUT3 to glucose is necessary to meet the strict and constant energy demands of the brain [7, 8].

GLUT2 is the most expressed transporter in the liver and is responsible for the transfer of glucose at the interface of liver and blood. Additionally, GLUT2 is an important glucose transporter in the intestine, where glucose enters the cell through the apical side of the intestine with SGLT1 transporters. It leaves the cell through GLUT2 transporters at the basolateral side and is co-dependent with the glucose uptake of SGLT1 [35, 36]. The process is sketched in Figure 1.5 for a better understanding. GLUT2 is responsible for glucose uptake and release in the liver, but studies show that it is not essential for the release of glucose since there exist an alternative way from hepatocytes [37].

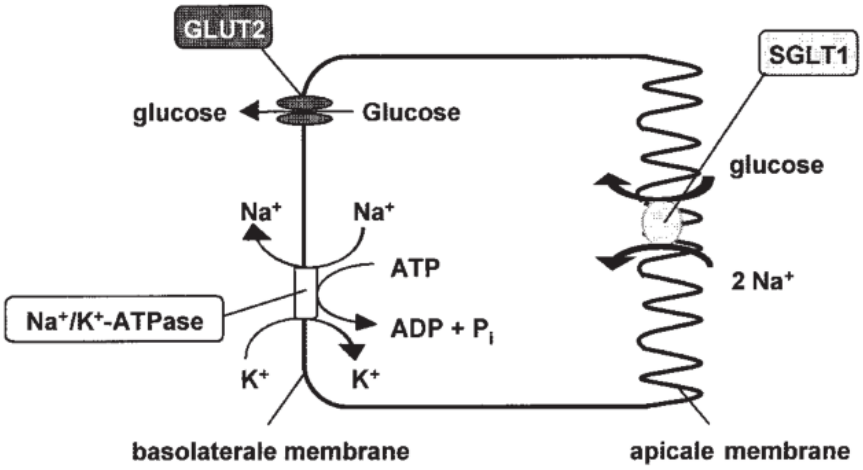

Figure 1.5: Image of GLUT2 as a transporter at the basolateral side of the intestine. Glucose enters the cell with SGLT1 transporters at the apical side of the cell and exits it via GLUT2 at the basal side. Picture derived from [36].

Table 1.1: The subtypes of the GLUT family with their respective functions, tissue distributions and known linked diseases in humans. Initial table from [27], additional information derived from [12, 38-41].

GLUT member	Function	Tissue distribution	Linked diseases
GLUT1	Glucose transport	Brain, blood-brain barrier, blood-tissue barrier, many fetal	Paroxysmal exertion-induced dyskinesia, dystonia-18, Glut1 deficiency syndrome
GLUT2	Glucose and fructose transport, glucose sensor in islet of Langerhans	Liver, intestine, kidney, brain, islet of Langerhans, lung	Fanconi-Bickel syndrome, type 2 diabetes
GLUT3	Glucose transport	Brain (neuronal), testis	-
GLUT4	Controls glucose uptake, insulin dependent	Adipose tissue, skeletal and cardiac muscle	Type 2 diabetes
GLUT5	Fructose transport	Small intestine, kidney, placenta	-
GLUT6	Glucose transport	Brain, spleen	-
GLUT7	Glucose and fructose transport	Small intestine, colon, testis, prostate	-
GLUT8	Glucose transport	Testis, brain, liver, spleen, heart brown adipose tissue, lung (intracellular)	down-regulated in testicular carcinoma
GLUT9	Urate transporter for glucose and fructose (electrogenic)	Kidney, liver, small intestine, placenta, lung	Renal hypouricemia
GLUT10	Glucose transport	Heart, lung, brain, liver, skeletal muscle, pancreas, placenta, kidney	Arterial tortuosity syndrome
GLUT11	Muscle-specific glucose and fructose transport	Heart, muscle	-
GLUT12	Glucose sensing, glucose transport	Heart, prostate, skeletal muscle, placenta, adipose tissue	-
GLUT13/HMIT	H^+/myo-inositol co-transporter	Brain, adipose tissue	-
GLUT14	Function related to spermatogenis	Testis	-

The member GLUT5 is a transporter specific for fructose and controls the fructose uptake in the small intestine through the apical membrane [42]. GLUT7 is a high affinity transporter for glucose and fructose where both measure a Km of 0.3 mM. It is expressed predominantly in organs such as the small intestine, colon, prostate and testis [43]. The facilitate transporter GLUT8 has a high affection for glucose with a Km of about 2mM. It can be inhibited by fructose. The main expression is localized in the intercellular compartment of the testes and brain and in lower amounts in liver, heart and intracellular lung. An exclusive feature of GLUT9 is that it is a urate glucose transporter, the transport is not dependent on the concentration of glucose but on the membrane potential. It has two isoforms, in liver and kidney both types GLUT9a and GLUT9b are present, while GLUT9a is also found placenta, pancreas, testis and more.

GLUT10 is a glucose transport protein and has its occurrence in many tissues including lung, placenta, liver, kidney, brain and pancreas [27]. Defects in gene sequence of GLUT10, SLC2A10, are the cause of arterial tortuosity syndrome [27, 44]. In the lung, the high affinity transporter GLUT10 together with GLUT2 controls the glucose uptake at the apical side of the membrane. Whereby the basal transport is regulated by GLUT1 and GLUT2. The combination of high affinity transporters on the apical and low affinity GLUTs on the basal side is beneficial for the apical to basal glucose transport, even on low glucose concentrations. It is suggested that the configuration is part of a lung defence mechanism to keep glucose concentrations in the lung and the possibility of spreading infections low [12].

The insulin dependent transporter GLUT4 is mainly found in skeletal muscle, adipose and cardiac tissues. It is known to have a major role in diabetes mellitus type II as it functions as an insulin-sensitive transporter. Insulin recruits GLUT4 so glucose is transferred from the blood through the membrane of these tissues. Otherwise, chronically high blood sugar levels could lead to heart diseases or kidney failures. In case of a defective expression of the transporter GLUT4, the diffusion of glucose is restricted into the cell. Although GLUT4 is known to be the primarily expressed insulin-dependent glucose transporter, studies suggest that insulin could stimulate the translocation of GLUT12 in skeletal muscle tissues. GLUT12 is also expressed in small intestine, and prostate, but acts as a non-insulin dependent transporter in the heart [27, 45].

1.2.2.2. The SGLT transport family

The SGLT transporter family is different from the GLUT family with respect to their substrate specificity, tissue distributions and, as already mentioned, transport mechanism. The family consists of six members, which operate with different kinetic properties as they are based on

secondary active transport. They co-transport sodium ions with glucose molecules against the glucose gradient. Table 1.2 summarizes the tissue distributions, functions and linked diseases of the SGLT subtypes.

Table 1.2: The subtypes of the SGLT family with their respective function and tissue distribution. Initial table from [28] with further information from [4, 36].

SGLT member	Function	Tissue distribution	Linked diseases
SGLT1	Glucose and galactose transporter	Intestine, trachea, kidney, heart, brain, testis, prostate	-
SGLT2	Glucose transporter	Kidney, liver, thyroid, muscle, heart	Type 2 diabetes
SGLT3	Glucose sensor in gut and brain	Intestine, spleen, kidney, muscle, testis, uterus, lung, brain, thyroid	-
SGLT4	-	Intestine, kidney, liver, brain, trachea, lung, uterus, pancreas	-
SGLT5	Glucose and galactose transporter	Kidney, cortex	-
SGLT6	Myo -inositol transporter	Spinal cord, kidney, brain	-

As a summary all the relevant glucose transporters of the placenta, lung, liver and intestines are pictured in Figure 1.6.

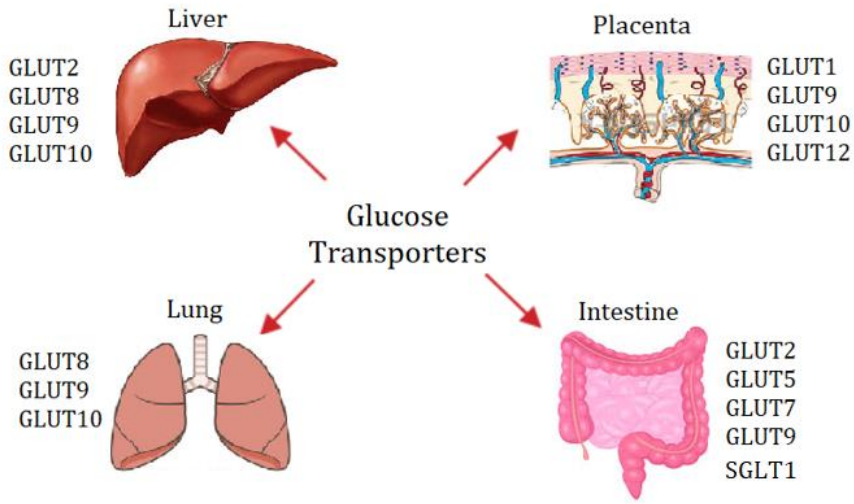

Figure 1.6: Summary of GLUTs in healthy human organs of liver (picture from [46]), placenta (picture from [47]), lung (picture from [48]) and gut (picture from [49]).

The most well-known sodium dependent glucose transporter is SGLT1. SGLT1 is primarily found in the intestines and the kidney and has a high affinity for glucose [4]. SGLT2 plays an almost

exclusive role in the kidney, but has also tissue occurrences in liver, thyroid, muscle and the heart. SGLT1 and SGLT3 transports glucose and sodium with a ratio of 1:2, and SGLT2 with a transport ratio of 1:1 [28, 36]. SGLT3 is more believed to be a glucose sensor rather than have a transport function. High expressions can be found in intestine, muscle and testis. Lower amounts of SGLT3 mRNA can be seen in heart, brain, uterus, lung and thyroid [50].

1.2.3. Cancer, glucose and the Warburg effect

Oxidative phosphorylation (OXPHOS) is a process in which energy is gained by the oxidation of nutrients to produce adenosine triphosphate (ATP). OXPHOS is carried out in the mitochondria. It is the main pathway for energy production in healthy cells if sufficient oxygen is available. If the oxygen supply is limited, ATP must be generated via anaerobic glycolysis, which is performed in the cytoplasm. Anaerobic glycolysis leads to lactate production, is less efficient than OXPHOS and produces 2 ATP per glucose instead of up to 36 ATP per glucose by its aerobic counterpart [51].

If enough oxygen is present, usually 70% of the ATP formation from glucose in healthy cells is produced by OXPHOS. However, tumour cells prefer glycolysis and less OXPHOS to produce energy, even under aerobic conditions to maintain cellular functions. The favoured aerobic glycolysis of tumour cells was first characterised by Otto Warburg and is termed the Warburg effect [52, 53]. But they are not retrieving their energy entirely by glycolysis, only up to 50-60%, and oxidative phosphorylation remains still important in some cancer types [54]. The Warburg effect leads to differences between the energetic metabolism in healthy and cancerous cells and therefore to differences in allocations and occurrences of glucose transporters. The preference of glycolysis in cancer cells has the consequence of abnormal up-regulation of GLUT1 [55, 56]. Thus GLUT1 is not only expressed in healthy tissue, but is overexpressed in particular cancer cell lines to deliver the additional energy they need for their rapid cell proliferation [40]. Accordingly GLUT1 is important in many cell lines used in research, as many of them are cancer cell lines [30]. All cancer cell lines studied in the current thesis have extremely up-regulated GLUT1 expressions.

GLUT1, 2 and 8-10 are the naturally expressed glucose transporters in human lung tissue [12, 27]. The insulin dependent GLUT4, which mainly controls glucose uptake in muscle and adipocytes, see

Table 1.1, is normally not expressed in healthy lung tissue. However, GLUT4 is found in the human adenocarcinoma cell line A549 [56]. Also mRNA levels of GLUT1, 3 and 12 were identified in this lung cancer cell line [57].

Among all GLUTs, GLUT2 is the dominating facilitate transporter in the human liver. Behind GLUT2, GLUT10 is expressed as the second highest transporter, followed by GLUT9 and GLUT8. In contrast, GLUT1 is by far the major transporter in Hep G2 cells, while GLUT2 seems comparatively uninteresting and is even outranked by GLUT3 [58].

In the human placental barrier GLUT1 is the primary transporter and in charge of glucose movement from the maternal to the fetal side [59]. Additionally, GLUT3 is transporter found in the early phase of pregnancy to guarantee enough glucose transfer to the fetus. GLUT9, GLUT10 and GLUT12 are also distributed in placental tissue [27]. [27]. In BeWo b30, GLUT1 and GLUT3 are both important glucose transporters as the cancer cell line origins from first trimester of pregnancy. GLUT3 is supposed to mediate 50% of glucose uptake in BeWo b30 cells [34, 60].

The Caco-2 cell line is colon cell line with a lot of transporters and enzymes that are found in normal intestine too. However, they also differ significantly in their in gene expression from normal intestinal epithelium [61]. Typical carriers for healthy colon tissue are GLUT1 and GLUT7. The cell line Caco-2 is often used as model for the intestine, but is originally a colon carcinoma cell line. GLUT5 is usually a fructose transporter found in the small intestine, but could be identified in the colon cell line Caco-2, as well as GLUT1 [62]. GLUT2, a popular transporter in the intestine, plays also a major role in the absorption of glucose [63].

The colorectal adenocarcinoma line HT-29 also shows a high expression of GLUT1 [64]. The transporter GLUT2, 3 and 5 were detected in the cell line as well [65]. In addition to facilitate glucose transporters, Caco-2 and HT-29 cells hold receptors for the active glucose transporter SGLT1. The extent of SGLT1 expression, however, is highly dependent on the place of cell line origin [66]. The distribution of the above-mentioned GLUTs in all laboratory cancer cell lines are summarised in Figure 1.7.

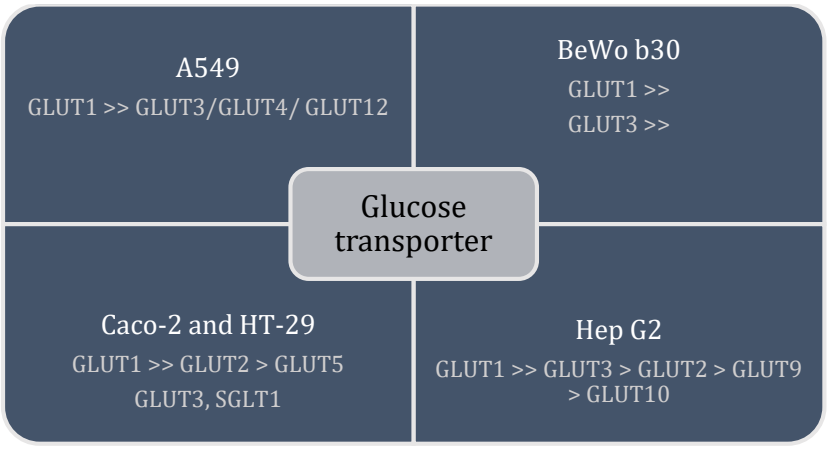

Figure 1.7: Summary of GLUTs in the laboratory cell lines in this work: A549, Hep G2, BeWo b30, Caco-2 and HT-29. GLUTs are ranked in priority if possible.

Caco-2 and HT-29 cells are both intestinal carcinoma cells, but Caco-2 cells differentiate toward absorptive and HT-29 toward mucus-secreting enterocytes. Together they can build a better and more physiological example of the human intestine [67].

1.2.4. Mechanisms of inhibition in glucose transport

In theory, all facilitate transport activities are saturable and are able to be restricted by competitive inhibitors [2]. The most prominent transporter GLUT1 can be inhibited by cytochalasin B (CB), phloretin (PT) and WZB-117 [30, 68].

The substance cytochalasin B, a mycotoxin found in apples, is a potent inhibitor for facilitate transporters. It interacts with the endofacial (export site, efflux) sugar binding site of GLUTs, which makes it a competitive inhibitor in glucose release, but non-competitive in glucose uptake [68]. It can bind to most of class I and class III family members, but does not have the appropriate binding site for GLUTs of class II. More precisely, CB blocks the subtypes GLUT1 [69], GLUT3, GLUT4, GLUT8 and GLUT12. CB exhibits low affinities to GLUT6 and HMIT [30]. Glucose transfer with GLUT2 is not inhibited by cytochalasin B [70]. Conversely, the compound WZB-117 binds to the exofacial (import site, influx) sugar binding site and acts competitive in the entry and non-competitive in the exit of glucose. WZB-117 is mainly known to be an irreversible GLUT1 inhibitor, but it was shown to block GLUT3 and GLUT4 as well. In order of strength, WZB-117 blocks GLUT4 strongly, followed with the similar inhibition strength of GLUT1 and GLUT3 [68].

The inhibitor phloretin, a phenol extracted from apples and pears [71], it also believed to work at the exofacial site of sugar transporters [72]. Phloretin interacts with the members GLUT1 [69], GLUT3 [73], GLUT4 [74], GLUT10 [75] and has a low affinity to HMIT [30]. It can strongly inhibit GLUT2 [76], but only partially GLUT9a. GLUT5 or GLUT7 are not inhibited by phloretin [30]. Phloretin is the non-sugar component of phlorizin (PZ). Phlorizin directly inhibits the co-transport in intestinal glucose absorption by binding to SGLT1 and SGLT2. Inhibition constants Ki of 0.2 μM for SLGT1 [77], 65 nM for SGLT2 [78] and 120 μM for SGLT3 [79] can be assigned to phlorizin (SGLT2>SGLT1>SGLT3). Lower inhibition constants Ki signify higher affinities to the SGLTs. Most studies portray phlorizin as a potent SGLT1 and 2 inhibitor with no influence on GLUTs, and its aglycon phloretin as a GLUT inhibitor with no affinities to SGLTs [80, 81]. In the studies of Kellet et al. [82, 83], the mechanisms responsible for intestinal glucose absorption in rats was investigated. As already discussed, GLUT2 is the most important transporter for the intestinal glucose absorption. It facilitates the exit of glucose through the basolateral membrane, while glucose is entered with the help of SGLT1 on the apical side [36]. A visualisation is provided in Figure 1.5. In Kellet & Helliwell's experimental design the glucose absorption was inhibited by

phloretin [82]. They concluded that the glucose absorption in the intestine is three times higher due to GLUT2 expression, because they assumed phloretin was only sensitive to GLUT2 and not SGLT1. It was later revealed that phloretin is a non-competitive inhibitor of SGLT1 with a Ki of 50 µM and they underrated the importance of SGLT1 expression in the intestine. However, the inhibition constant, Ki, for phloretin is 250 times higher than for phlorizin. Phloretin has an inhibition constant Ki of 50 µM, whereas phlorizin reveals an inhibition constant Ki of 200 nM [78]. Figure 1.8 visualizes the inhibition range of facilitate glucose transporters by cytochalasin B, phloretin and WZB-117.

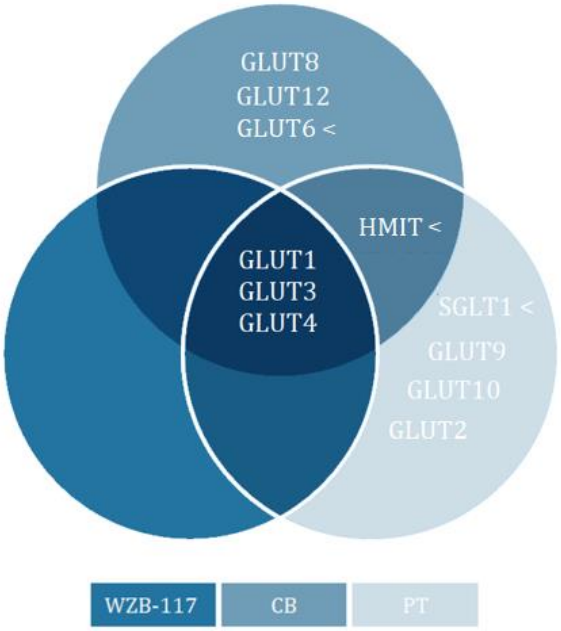

Figure 1.8: Range of inhibition of WZB-117, CB and PT in regard to GLUTs and SGLTs. Not mentioned transporters are not inhibited by the three inhibitors.

1.2.5. Detection of glucose with Fourier-transform infrared spectroscopy

The quantification of glucose is a vital part for the assessment of cell functionality and monitoring of transport processes by cell barriers. However, it is not only important topic in the current work, but also an ongoing field of research. Especially Fourier-transform infrared (FTIR) spectroscopy has been proven to be a fast and label-free method to detect glucose. It can be used for the measurement of glucose in blood, serum or other body fluids [84]. Given the importance of daily glucose measurements for diabetic patients, non-invasive glucose measurements applying infrared (IR) spectroscopy are also under development [85]. Other purposes arise in applications in the food or the agriculture industry as a quality control measure [86]. The examination of

inelastic scattering of light on molecules in Raman spectroscopy is a further method for reagent-free glucose analysis. An advantage over infrared spectroscopy is that the spectrum of water is weaker in Raman spectra. However, the Raman effect itself is weak and can be masked by fluorescence of the samples [87].

Table 1.3: Advantages and disadvantages of Raman spectroscopy, infrared spectroscopy and colorimetric assays. Information about electrochemical glucose sensing from [88]

Technique	Advantages	Disadvantages
Raman spectroscopy	Label-free Fast measurement Minimum sample preparation Non-invasive Weak absorbance of water Excitation wavelength can be chosen Reagent-free	Interference from fluorescence Measurement of multiple analytes Raman effect is weak
Infrared spectroscopy	Label-free Fast measurement Minimum sample preparation Non-invasive Reagent-free Measurement of multiple analytes	Strong spectrum of water
Colorimetric assay	Specific detection of glucose High sensitivity	Requires reagents High turnover rate Sample preparation required Influenced by many factors (e.g. temperature, pH)
Electrochemical detector	Not dependent on glucose oxidase Low limit of detection Sensitivity and selectivity Minimal affected by temperature	Surface reactions

An alternative to spectroscopy is provided by enzymatic analysis methods, which allows specific detection of glucose with colorimetry. In case of the colorimetric technique, a glucose enzyme mix oxidizes glucose in the sample by glucose oxidase to hydrogen peroxide and gluconolacetone, which reacts with a dye and generates a colour that can be detected at a certain wavelength. The fluorescence intensity of the colour is proportional to the amount of glucose in the sample. This technique is specific for glucose and insensitive to other reducing sugars [89].

Within this work, it was shown that the acquired FTIR absorbance data behave equally proportional to the glucose concentrations as in the colorimetric approach within the investigated concentration region of 0.01 and 4.5 mg/ml. Advantages of the proposed FTIR approach are the minimum required sample preparation and a fast measurement compared to colorimetric glucose assays. In this work the standard colorimetric approach was employed to validate the quality of the FTIR-based measurement method. A comparison between different techniques for glucose detection is listed in Table 1.3.

1.2.5.1. Fundamentals of infrared spectroscopy

Infrared spectroscopy is a technique for the identification and quantification of unknown substances in the sample. First, the basic principles of absorption spectroscopy are explained. For the observation of a spectrum, the transmittance of a sample with electromagnetic radiation can be measured as a function of the wavelength. The transmission of a medium is defined as the ratio of transmitted and penetrated beam power. The schematic structure and important components of an IR spectrometer can be seen in Figure 1.9.

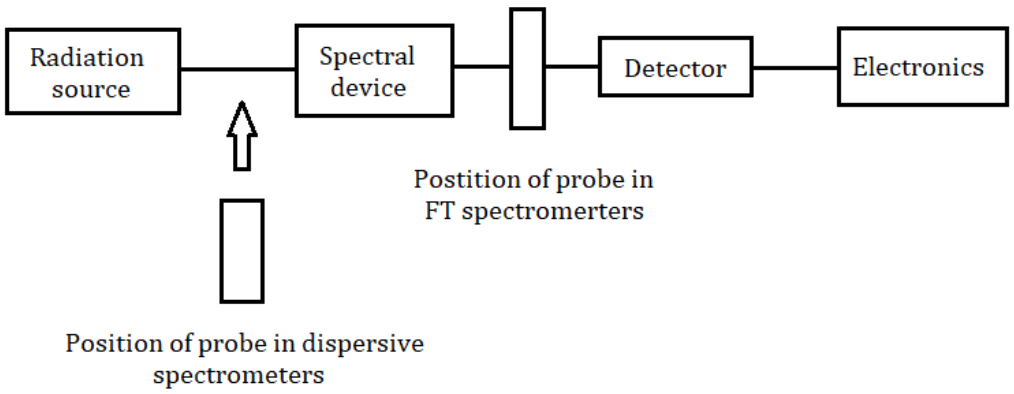

Figure 1.9: Schematic structure and components of an IR spectrometer. Picture from [90].

The first component in absorption spectroscopy is the radiation source. It should have the highest possible intensity in the wavelength range of interest. In most cases thermal radiators are used, which provide broadband radiation. Another important element is the spectral device, which separates the spectrum into defined spectral ranges. Based on the spectral device, a distinction is made between non-dispersive, dispersive and Fourier-transform (FT) spectrometers. In non-dispersive spectrometers variable wavelength selection is not possible. In FT spectrometers, the spectral separation is performed with an interferometer, which enables wavelength-dependent modulation. Mostly Michelson interferometers are used, in which two-beam interferences are

converted into spectral information by Fourier transformation. Dispersive spectrometers use spectral devices for variable wavelength selection such as prisms. In dispersive spectrometers the probe is placed before the spectral device in order to be able to eliminate the scattered light caused by the probe. In case of FT spectrometers the probe is arranged after the spectral device, so that the emitted sample radiation remains unmodulated. The function of the optical system is the loss free transfer of the radiation from the radiation source to the detector. In IR spectrometers the optical system is equipped with mirror optics. A detector converts the optical signal into a measurable electrical signal. Afterwards, the signal from the detector is amplified and digitalized by appropriate electronics.

A non-destructive measurement technique, attenuated total reflection (ATR), measures the IR spectrum at the surface of a probe. It is based on the phenomena of light reflection at the interface of two media with different refractive indices. The total reflected radiation in the medium with the higher refractive index (crystal) penetrates some wavelengths deep into the optically thinner medium (probe). In order to achieve a total reflection, the angle of incidence at the interface between sample and the crystal must be greater than the critical angle of the total reflection. (1.1) shows the relationship of the critical angle θ_C, the refractive index of the ATR crystal n_1 and the refractive index of the sample n_2.

$$\theta_C = \sin^{-1}\frac{n_2}{n_1} \tag{1.1}$$

The intensity of the radiation in the optically thinner medium decreases with the distance from the surface of the internal reflection element. The penetration depth into the optically thinner probe measures only a few wavelengths. Therefore, a huge advantage of the ATR spectrum is that it is usually independent of the sample thickness. Even thick and strongly absorbing samples can be analyzed [90].

The entire infrared spectrum is divided in three regions:

(1) Far infrared (< 400 cm^{-1})
(2) Mid infrared (4000 - 400 cm^{-1}) and
(3) Near infrared (14285 - 4000 cm^{-1}) region

The regions of the spectra are given in inverse wavelengths, referred to as wavenumber scale in the unit cm^{-1}. The relationship between the wavenumber k and the wavelength λ is given in the Equation (1.2). The final absorbance spectrum of IR spectroscopy plots the absorbance value in arbitrary units (a.u.) against the wavenumber (cm^{-1}).

$$k\ (cm^{-1}) = \frac{1}{\lambda\ (cm)} \tag{1.2}$$

The absorbance of an analyte is directly proportional to its concentration. The absorbance, denoted as A, is defined as the negative logarithm of the transmittance, denoted as T. Their relationship is given in Equation (1.3).

$$\mathrm{A\ (a.u.)} = -\log \mathrm{T} \tag{1.3}$$

The transmittance determines the ratio of the intensity of sample solution, I_S, to the intensity of a reference solution, I_R, as in the Equation [22].

$$T = \frac{I_s}{I_R} \tag{1.4}$$

1.2.5.2. Spectrum of glucose in infrared spectroscopy

In infrared spectroscopy, atoms of molecules vibrate or rotate when they are excited by frequencies in one of their fundamental modes. The vibrational motion of a small part of the molecule is triggered, whereas the rest is unaffected. A vibration can either include an alteration in the length of a bond, known as stretching, or a change in the angle of a bond, called bending. Stretching vibrations can be symmetrical or asymmetrical [22]. Examples for stretching and bending vibrations are shown in Figure 1.10.

The discrete frequencies of glucose at specific energies are identified by the mass and vibrational bond of the atoms [91]. The mid-infrared region is particularly interesting for the detection of glucose, as the fundamental frequencies of glucose are settled in the region of 4000-900 cm^{-1}. The spectrum of glucose consists of several local maxima in the spectrum which are corresponding to the stimulation of the vibrational modes of the OH and CO groups. It is an accumulation of different (as)-symmetric and vibrational modes of the glucose structure [22].

The fundamental frequencies of glucose result from the chemical composition of glucose. Its cyclic structure is shown in Figure 1.2. Because of its 6 membered hemiacetal ring structure, D-glucose is also known by D-glycopyranose, after the heterocycle pyran. D-glycopyranose is a stereoisomer and can form α- or β-anomers through their open chain form. If D-glucose is dissolved in water, α- and β- anomers of D-glucose interconvert until an equilibrium is found. This interconversion called mutarotation occurs by the way of their open-chain aldehyde form. The equilibrium of D-glucose is found in their 0.02% open chain form, 36% α-D-glucose and 64% β-D-glucose [92]. The open chain form of glucose does not produce a significant signal in the spectrum, as its aldehyde group would trigger carbonyl absorption [22].

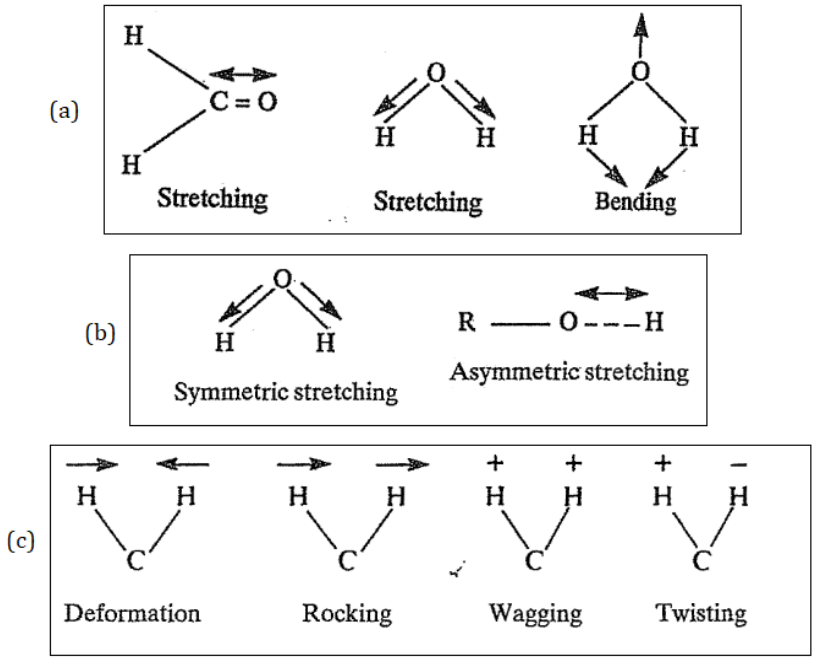

Figure 1.10: (a) Examples of stretching and bending vibrations. (b) Examples of symmetric and asymmetric stretching vibrations. (c) Examples of bending vibrations. Pictures derived from [22].

The spectra and corresponding assignments of glucose which are calculated based on a model of band positions of glucose are given in Table 1.4. In contrast to the modelling calculation of glucose spectra, the experimental infrared spectroscopy displays vibration signals of CO and CC groups from 600 – 1500 cm^{-1}, vibrations of CH and OH groups are located from 2900 – 3250 cm^{-1} and vibrational CH and OH groups are settled from 2900 – 3450 cm^{-1} in the spectrum [93]. Infrared spectroscopy can quantify multiple analytes in the same spectrum with a single measurement. In order to find out the concentration of a single compound in a solution, a reference or calibration graph is first needed and evaluated at a given infrared wavelength. With the reference curve it is then possible to analyse the concentration of the compound of interest at the same wavelength.

Table 1.4: Infrared frequencies and assignments of glucose are located in the mid infrared region. Information from [93].

Frequency (cm^{-1})	Assignments
3876 – 3005	OH stretching
<2061	CH vibrations
1849 – 1634	C=O stretching
1526 – 1347	OCH/COH deformation
1362 – 1191	CH/OH deformation
1191 – 995	CO and CH stretching

1.3. Research objectives

In the current work the comparative characterisations of five distinct organ systems in regard to transport processes of glucose are discussed. In every organ, specific passive GLUTs and/or active sodium-dependent glucose SGLT transporters are responsible for the transfer of glucose. The specific organ barriers include the lung, placenta, liver and intestines, which are represented by the human cancer cell lines A549, BeWo b30, Hep G2 and Caco-2/HT-29 in in-vitro models respectively. In these models, cells of the according organ are seeded permeable membranes to develop a cell-monolayer. In doing so, they exhibit physiological attributes which are comparable to organ barrier functionalities [14]. Based on the cell monolayers, comparative transport studies of glucose were performed for each organ cell line. Prior, the integrity and function of the cell barriers were assessed and evaluated with the monitoring of the transepithelial/endothelial resistance (TEER) and sodium fluorescein leakage (Na-flu) assays.

As main part of the study the influence of the inhibitors cytochalasin B, phloretin and WZB-117 on glucose transfer was investigated. The impact of single glucose transporters and their inhibition in each human barrier was compared and discussed. The measurement and acquisition of glucose was assessed with vibrational infrared spectroscopy. Additionally, the infrared absorbance spectrum and eigenfrequencies of glucose were evaluated and a calibration of glucose detection was performed. On the basis of the calibration, the glucose concentrations during the transport experiments were determined.

2. Materials and Methods

2.1. Cell culture

The human placental cell line BeWo b30 was cultured in equal amounts of high glucose Dulbecco's Modified Eagle Medium ($DMEM_{HIGH\ GLUCOSE}$) (Sigma Aldrich, Cat. nr. D6429) containing 4.5 mg/ml glucose, or 25 mM respectively, and Ham's Nutrient Mixture F12 (Sigma Aldrich, Cat. nr. 51651C) with 10% fetal bovine serum (FBS) (Sigma Aldrich, Cat. nr. F0804) and 1% antibiotics (AB) (Sigma Aldrich, Cat. nr. A5955). The cellular intestinal models Caco-2 and HT-29 cells were maintained in DMEM with 10% FBS, 1% antibiotics and additionally 1% non-essential amino acids (NEAA) (Gibco, Cat. nr. 11140-035). The human liver cancer Hep G2 cells were cultured in modified Eagle's medium (MEM) (Sigma Aldrich, Cat. nr. M4526), 10% FBS and 1% antibiotics. The alveolar cell line A549 was cultivated in Roswell Park Memorial Institute (RPMI) (Sigma Aldrich, Cat. nr. R8758) with 10% FBS and 1% antibiotics.

The medium was refreshed every 2 to 3 days and cells were split when they reached 80% confluence. The cells were maintained in an incubator at 37°C and under 5% carbon dioxide (CO_2) in air.

2.2. Glucose transport and uptake studies

2.2.1. Transwell culture of transport cell barrier models

The transport and uptake processes were performed with the lung barrier A459, the placental barrier BeWo b30, the hepatic barrier Hep G2, the intestinal barriers Caco-2 and HT-29 and a co-culture with 90% Caco-2 and 10% HT-29.

The cells were seeded onto porous polyester transwell membranes for barrier integrity and glucose transport studies. The inserts had a growth area of 1.2 cm^2, a pore size of 3.0 µm and were designed for 12-well tissue culture plates. The cells were seeded with a density of 1 x 10^5 cells/cm^2 on the apical side of the permeable membrane inserts on day 0. The apical chamber was filled with 0.5 ml and the basal compartment with 1.5 ml of the appropriate cell culture medium for each cell type. For the no-cell controls, the respective amount of cell culture medium was filled in the apical and the basal chambers. The medium was refreshed every second day (on day 1, 3, 5 and 7 post seeding).

2.2.2. Evaluation of the barrier integrity

2.2.2.1. Monitoring of trans-epithelial resistance (TEER)

All trans-epithelial resistance measurements were performed with the STX2 electrode pair of the epithelial EVOM2 voltmeter (World Precision Instruments Ltd). The outer longer electrode touched the bottom of the culture plate and the shorter inner electrode was placed in the apical chamber of the transwell insert, which was placed in 12 well tissue culture plates, to ensure reproducible electrode-to-membrane distances. TEER was measured and averaged at three different points with an angle of 120° to each other in every transwell. Electrodes were immersed in cell culture media before measurements for about 30 minutes, while the device was in operation mode. TEER measurements were performed after medium replacement and sample cool-down to room temperature. The EVOM2 measures the total resistance, referred to as R_{TOTAL}, where the resistance of the blank transwell membrane, denoted as R_{BLANK}, is subjoined to the total resistance. Therefore, the resistance value of no-cell inserts is subtracted from the TEER values to obtain the true tissue resistance, as seen in Equation (2.1).

$$R_{TRUE\ TISSUE}\ (\Omega) = R_{TOTAL}\ (\Omega) - R_{BLANK}\ (\Omega) \quad (2.1)$$

The resistance $R_{TRUE\ TISSUE}$ is inversely proportional to the area of the cell tissue. Thus, the concept of the unit area resistance, $R_{UNIT\ AREA}$, is used. It is the product of the true resistance, $R_{TRUE\ TISSUE}$ in Ω and the area of the well, A_{WELL} in cm^2 given in $\Omega*cm^2$. The relationship is shown in Equation (2.2).

$$R_{UNIT\ AREA}\ (\Omega * cm^2) = R_{TRUE\ TISSUE}\ (\Omega) * A_{WELL}\ (cm^2) \quad (2.2)$$

Main advantage of unit area resistance is its independency of the area of the membrane and that transwell inserts of different sizes are comparable. Therefore, unit area resistance was used in TEER data representation within this work [94].

2.2.2.2. Sodium-fluorescein leakage assay

For additional evaluation of barrier integrity based on non-electrical means, a sodium fluorescein leakage assay was performed on the transwell cell- monolayers on day 3 and 7 post seeding. First the medium was removed from both apical and basal compartments. The basal chamber was filled with 1.5 ml of fresh medium and the apical side of the transwell with 0.5 ml of 5 µM sodium fluorescein (Sigma Aldrich, Cat. nr. F6377) in fresh medium. The transwells were incubated for one hour in the dark at 37°C. In the second step, 50 µl of apical and basal chambers was transferred into a 96-well tissue culture plate. The fluorescence was measured with an EnSpire 2300 plate reader (Excitation (Ex) 470 nm/Emission (Em) 525 nm; Perkin Elmer). Results show the relation between basal to apical fluorescence in percentage.

2.2.3. Cell viability

Cell viability experiments were carried out to assess the condition of the cell barriers at the time of the glucose transport and glucose inhibition experiments on day 8. For the metabolic assessment of the cell barriers over time, assay experiments with the cell viability reagent PrestoBlue™ (PB) (Invitrogen life technologies, LOT 1824890) were conducted for A459, BeWo b30, Caco-2, HT-29 and Hep G2. Therefore, each cell line was seeded with a density of $1 * 10^5$ cells/cm^2 on 48-well tissue culture plates on day 0. The medium was exchanged every second day, on day 1, 3, 5 and 7, before the experiments were conducted. PB was mixed in a ratio of 1:10 with fresh medium. The old medium was removed and the PB-medium mixture was added into the

wells (200 µl/well, 3 wells per cell line). As a control, PB was added to medium without cells referred to as blank (3 wells per cell line). The incubation time was 60 minutes in the dark at 37°C. Afterwards, 100 µl of the incubated solution was pipetted to a 96-well tissue culture plate in preparation for the fluorescence measurement with the EnSpire 2300 plate reader (Ex. 560 nm/Em. 590 nm; Perkin Elmer). The fluorescence values were averaged before determining the viability. The calculation of cell viability in percentage was carried out with the Equation (2.3).

$$\text{Metabolic rate (\%)} = \frac{\text{Sample at day x (x} = 1, 3, 5, 7) - \text{ Blank without cells}}{\text{Sample at day 1} - \text{Blank without cells}} * 100 \qquad (2.3)$$

For a visual control of viability, a live/dead staining of the cells occurred on the same days as for the PB experiments. The cells were treated with the reagents Calcein AM (CA AM) and Ethidium Homodimer-1 (EthD-1) (Invitrogen life technologies, LOT 1906259). The compounds were mixed with fresh media in ratios of 1:1000 for CA and 1:2000 for EthD-1. The old medium was removed and substituted by the staining solution, and afterwards incubated for 30 minutes in the dark at 37 °C. The images were taken with the live-cell microscope XXX with 20x magnification. Viable cells are shown in green (Ex. 495 nm/ Em. 515 nm for CA AM) and non-viable cells in red (Ex. 495 nm/ Em. 635 nm for Eth-D1).

2.2.4. Preparation of glucose inhibitors

The first inhibitor cytochalasin B from *Drechslera dematioidea* (Sigma Aldrich, Cat. nr. C6762) was dissolved in dimethyl sulfoxide (DMSO) (10.4 mM) with a final concentration of 20 µM in respective medium. Phloretin (Sigma Aldrich, Cat. nr. P7912) was dissolved in 99% ethanol (91 mM) and then further diluted with the respective cell culture medium to final concentrations of 1 mM and 30 µM. WZB-117, the GLUT1 inhibitor, (Sigma Aldrich, Cat. nr. SML0621) was dissolved in DMSO (67 mM) and thinned with respective medium down to 20 µM.

2.2.5. Glucose transport and uptake studies

Transport and uptake experiments were facilitated after conformation of cell barrier integrity and confluence as described in the methods above. Every transport and uptake experiments with and without glucose transporter inhibitors were performed at least three times.

A general characterization of the glucose transport and uptake of all five barrier models was carried out on day 7 post seeding. The apical chamber was filled with 0.7 ml of high glucose $DMEM_{HIGH\ GLUCOSE}$ and 1.5 ml of DMEM without glucose (Gibco, Ref. nr. 11966-02), referred to as $DMEM_{NO\ GLUCOSE}$, was sampled into the basal chamber of each transwell. A 50 µl sample of the apical and basal compartment was taken at the times of 0, 60, 105 and 150 minutes. The results were corrected for the removal of 30µl for each measurement time point. The no-cell controls were performed with the respective amount of $DMEM_{HIGH\ GLUCOSE}$ and $DMEM_{NO\ GLUCOSE}$ to monitor diffusion processes.

The basal glucose transport rate was calculated with the formula given in Equation (2.4). It describes the relation of differences in basal glucose concentrations, c_B, between two neighbouring time points to the according time difference.

$$\text{Transport rate } (t_n) = \frac{c_b(t_n) - c_b(t_{n-1})}{t_n - t_{n-1}} \text{ for } 0 < n < 4;\ t(n) = \{0\ , 1, 1.75, 2.5\}\ \text{h} \qquad (2.4)$$

The transport process is finished when an equilibrium of glucose concentration between the apical and basal chamber is achieved. The calculation of the equilibrium was determined according Equation (2.5). The results are corrected for volume loss of 50 µl at each measurement time point. The glucose concentrations in apical and basal compartment are referred to as c_A and c_B, and the corresponding volumes to V_A and V_B at a time.

$$\text{Equilibrium } (t_n) = \frac{V_A\,(t_n) c_A(t_n) + V_B(t_n)\, c_B(t_n)}{V_A(t_n) + V_B(t_n)} \text{ for } 0 \leq n < 4;\ t(n) = \{0\ , 1, 1.75, 2.5\}\ \text{h} \qquad (2.5)$$

To determine the roles of different GLUT transporter, the impact of three different glucose inhibitors were tested on glucose transport for the five cell barriers and the co-culture of the two intestinal barriers.

In the inhibition experiments, the cell barriers were treated with the GLUT inhibitors on day 7 post seeding and incubated for 24 hours in the dark at 37°C. The preparation of the agents is described above. The transport experiments were conducted on day 8 post seeding.

The apical chamber was filled with 0.5 ml $DMEM_{HIGH\ GLUCOSE}$ and the basal chamber with 1.5 ml $DMEM_{NO\ GLUCOSE}$. Samples of apical and basal compartments were taken after 1 hour for cells treated with CB and after 2 hours for cells treated with PT or WZB-117. The results of glucose transport inhibition is given in percentage of the untreated cells (controls).

2.2.6. Effect of cell apoptosis and necrosis on glucose transport and infrared spectrum

To determine the impact of cell apoptosis and necrosis on the IR spectrum of glucose and on glucose transport, the effect of high dosage PT was tested. Similar to the inhibition experiments, the cell barriers were treated with 1 mM phloretin on day 7 post seeding and incubated for 24 hours in the dark at 37°C. The transport experiments were conducted on day 8 post seeding.

The apical chamber was filled with 0.5 ml $DMEM_{HIGH\ GLUCOSE}$ and the basal chamber with 1.5 ml $DMEM_{NO\ GLUCOSE}$. Samples of apical and basal compartments were taken after 1 hour for cells treated with PT.

2.2.7. Detection of glucose

Infrared spectroscopy, as well as colorimetric glucose detection, are comparative measurement techniques which require a standard reference within the analytical process. Therefore, it is necessary to perform a reference measurement series with which the actual glucose measurements are analysed. In this work, the colorimetric determination of glucose served as a comparison to the infrared spectroscopy and as a validation for the quality of the FTIR method.

2.2.7.1. Infrared spectroscopy

Infrared spectroscopy was measured with a platinum ATR sampling unit on an InfraRed Bruker Tensor 37. The manipulation of the graphs was performed with OPUS 7.5® software. The measurements were recorded with an average of 200 scans at 2 cm^{-1} resolution. The recorded measurement region covered the mid infrared region from 4000 – 900 cm^{-1}. The absorbance spectrums were smoothed with 9 smoothing points and integrated. The height integration method included a baseline correction.

A 30 µl sample was pipetted onto the diamond ATR crystal, which was cleaned with ethanol before each measurement. For the reference series, the absorbance spectrum was analysed at the wavelengths of the fundamental vibrations of glucose at 1153 cm^{-1}, 1108 cm^{-1}, 1080.5 cm^{-1}, 1035.7 cm^{-1} and 994.3 cm^{-1} of the mid infra-red (MIR) region. For the rest of the glucose transport and

uptake studies the absorbance was analysed at the wavelength of 1035.7 cm^{-1}, if not stated otherwise.

Four different dilution series were prepared for the reference series to analyse the impact of different solvents in the absorbance spectrum. The reference sample, $DMEM_{HIGH\ GLUCOSE}$ solution was diluted down to 0.05 mg/ml with either $DMEM_{NO\ GLUCOSE}$, Dulbecco's Phosphate Buffered Saline (PBS) without calcium chloride ($CaCl_2$) and magnesium chloride ($MgCl_2$) (PBS-) (Sigma Aldrich, Cat. nr. D8537), with $CaCl_2$ and $MgCl_2$ (PBS+) (Sigma Aldrich, Cat. nr. D8662) or distilled water. Based on the reference series, a calibration in the form of the Equation (2.6) was used to determine the concentration of glucose in the transport and uptake studies. The response of the infrared spectrometer, *y*, was assumed to be a linear function of the reference glucose concentrations, *x*, where *k* is the slope and *d* the intercept of the calibration line [95].

$$y = kx + d \tag{2.6}$$

The sensitivity, or slope, *k* of linear regression was used for the calculation of the limit of quantification (LOQ) and limit of detection (LOD). The applied formula is given in the Equations (2.7) and (2.8).

$$LOD = 3\ \frac{\text{RMS noise}}{k} \tag{2.7}$$

$$LOQ = 10\ \frac{\text{RMS noise}}{k} \tag{2.8}$$

The root mean square (RMS) noise of the instrument was measured twice from 1200 to 990 cm^{-1} (with the same number of scans) and averaged and the slope of the calibration line was determined for each wavenumber.

2.2.7.2. Colorimetric glucose assay

For the colorimetric approach, the same range of glucose concentrations as for infrared spectroscopy was measured. The standard solution of the kit was prepared as per instructions given in the glucose assay kit (Abcam, *ab65333*). The measurement of standards, controls and samples were assayed in duplicate. The highest glucose concentration detectable by the kit is 200 µM (=36 $*10^{-3}$ mg/ml). For the reference series, first D-(+)-Glucose (Sigma Aldrich, Cat. nr. G5400) was dissolved in distilled water, to create sugar solutions with concentrations from 25 mM to 560 µM. Secondly, the whole reference series was diluted in a ratio of 1:130 to fall below the maximum

of 200 µM glucose in the standard series. Then, standard and samples (reference series) were pipetted into a 96-well tissue culture plate. For each measurement 50 µl of reaction mix was added into the standard and sample wells. Additionally 50 µl of background reaction mix was into background control wells. The plate was incubated for 30 minutes in the dark at 37°C and then analysed with the EnSpire 2300 plate reader (Ex. 535 nm/Em. 587 nm; Perkin Elmer).

3. Results and Discussion

3.1. Evaluation of barrier integrity

This section shows a comparative evaluation of five human in-vitro cell barriers in regard to the development of their barrier integrity. Depending on the type of organ barrier, substantial differences under the same conditions can be reported for the course and elevation of TEER values and sodium fluorescein leakage reduction.

3.1.1. TEER monitoring

Barrier integrity is important for the physiological functionality of the cell monolayers. One of the most common approaches to assess the functionality of an organ barrier is the measurement of the transepithelial/endothelial electrical resistance. Generally, the TEER measurement is a technique to measure the integrity of tight junction dynamics in in-vitro cell culture models of epithelial monolayers. The advantage of the transepithelial electrical resistance is that it is a label free measurement procedure of the barrier function, which can be recorded without damaging the cells [96]. In order to evaluate the integrity of the cell barriers A549, BeWo b30, Hep G2, Caco-2, HT-29 and Caco-2 & HT-29 co-culture the course of TEER was followed in a transwell set-up. The initial cell density was $1*10^5$ cells/cm^2 for each cell type and $9*10^4$ Caco-2/cm^2 with $1*10^4$ HT-29/cm^2 for the Caco-2 & HT-29 co-culture on day 0. TEER was measured every second day. The results of TEER in form of the unit area resistance measurements are shown in Figure 3.1 for all cell barriers. The unit area resistance on day 7 post seeding reached 125,20 ± 5,72 Ωcm^2 for A549, 119.47 ± 11.6 Ωcm^2 for BeWo b30, 80 ± 7.11 Ωcm^2 for Hep G2, 134.67 ± 7.68 Ωcm^2 for Caco-2, 101.33 ± 13.23 Ωcm^2 for HT-29 and 171.73 ± 7.26 Ωcm^2 for the co-culture of Caco-2 & HT-29. The average TEER value of the acellular controls amounts to 124.4 ± 21.46 Ωcm^2 for A549 culture medium, 140.1 ± 22.7 Ωcm^2 for BeWo b30 culture medium, 166.9 ± 21.2 Ωcm^2 for Caco2/HT-29 culture medium and 114.5 ± 12.7 Ωcm^2 for Hep G2 culture medium. The significant variances in TEER between different medium compositions clearly underline why the total resistance is less meaningful then the true tissue resistance and therefore most commonly used [14]. Overall, the co-culture of Caco-2 & HT-29 cells resulted in the highest increase in TEER, whereas the Hep G2 cell barrier reads the lowest TEER at day 7 and shows the overall lowest TEER development.

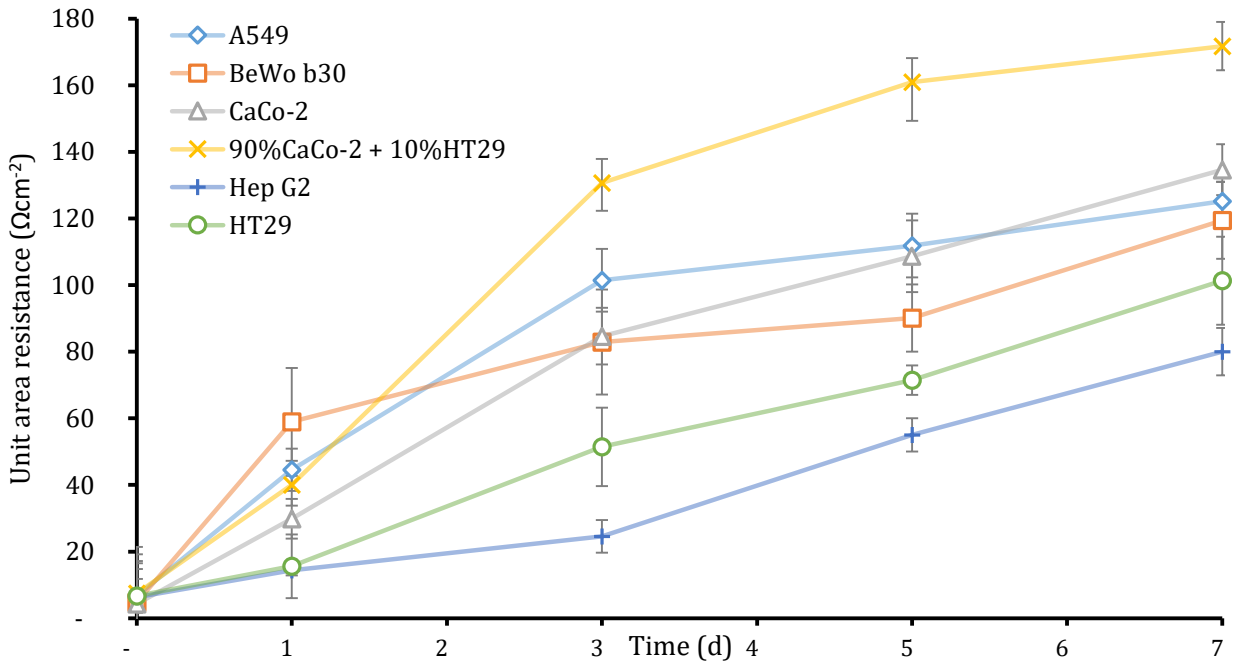

Figure 3.1: Barrier integrity based on the transepithelial electrical resistance of A549, BeWo b30, Hep G2, Caco-2, HT-29 and Caco-2 & HT-29 co-culture. The individual cell types were seeded in a transwell set-up with $1*10^5$ cells/cm² and the co-culture with a ratio of 90 %Caco-2 & 10% HT-29 at day 0. TEER was measured at day 1, 3, 5 and 7 post seeding after fresh medium exchange at room temperature and is given as unit area resistance in Ωcm².

Since TEER measures the ion flux through the epithelial barriers, it gives indirect information about the formation of electrically tight junctions. In this context electrically-tight means that the cells form confluent layers which prevent the passage of ion currents along their pathway. As the trans-cellular junction is formed by junctional proteins such as ZO-1, the epithelial electrical resistance raises. Therefore, the extent of cell tightness can be determined through the measurement of TEER [97].

In this context, the results indicate that the intestinal barrier Caco-2 and the co-culture of Caco-2 with HT-29 cells form a better cell barrier in terms of barrier tightness than the intestinal barrier HT-29, lung, placental or hepatic cell models. Although Caco-2 and HT-29 are both colon carcinoma cells, they show strong differences in their TEER development. Similar to differences in gene expression along the human intestinal tract, the colon carcinoma cells express dissimilarities in gene expression as well. Also, the intestinal tract is built on various types of cells. One cell type cannot represent the whole physiology of the intestine. Caco-2 cells express characteristics of colonocyte and enterocyte phenotypes and are known for high TEER values [98]. Whereas, HT-29 cells have goblet cell properties and produce lower TEER values, which are more physiological to in-vivo situations [61]. Furthermore, the BeWo b30 and A549 barriers show similar TEER readings. The hepatic barrier shows the smallest TEER and degree of tight junction formation in comparison to the other organ barriers.

A downside of the TEER technique is that it can have highly diverging results, even with the same cell lines. One reason for the variation of the TEER is that a minor defects in cell coverage or cell death due to cytotoxic agents can have a great effect on the measured TEER value [14, 99]. Therefore, the confluency and viability of all cell barriers was monitored additionally to ensure measurement of healthy cell barriers. All cell barriers achieved a confluent cell layer at day 3 post seeding, as shown in Figure 3.3 – Figure 3.7 (a). Additionally, every reading was performed under similar conditions to ensure data quality and prevent impaired readings.

3.1.2. Sodium fluorescein leakage

In the second part of ensuring an adequate physiological barrier, the sodium fluorescein leakage of all cell barriers were analysed during the formation of tight cell barriers. The sodium fluorescein leakage assay was performed in the same transwell system set-up as for the TEER measurements. The results of the Na-Flu leakage assay can be seen in Figure 3.2.

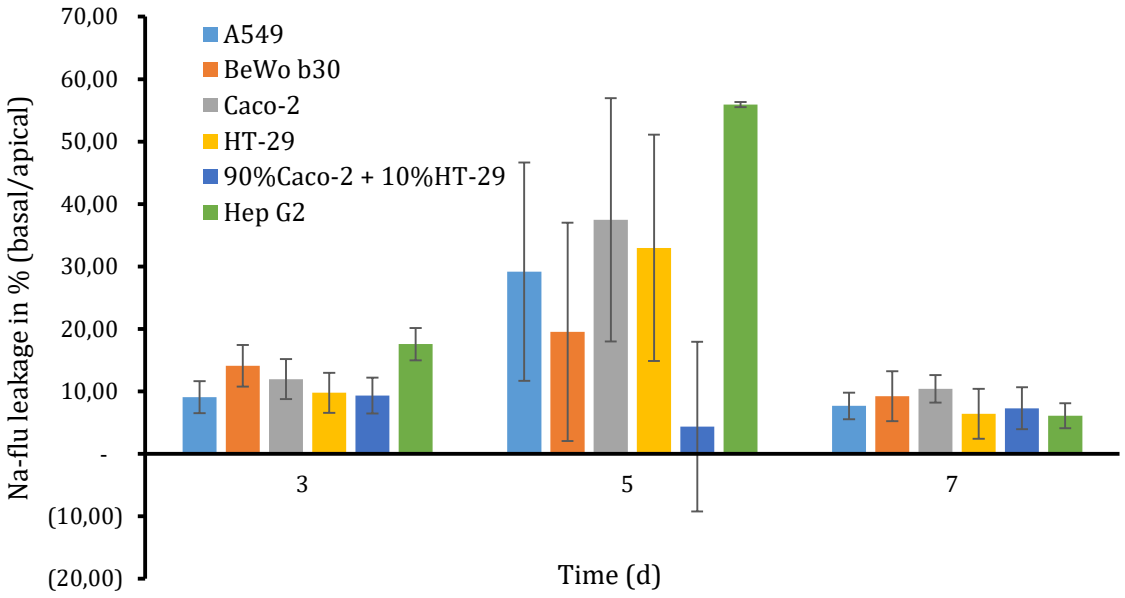

Figure 3.2: Barrier integrity based on the sodium fluorescein leakage of A549, BeWo b30, Hep G2, Caco-2, HT-29 and Caco-2 & HT-29 co-culture at day 3, 5 and 7 post seeding. The individual cell types were seeded in a transwell set-up with $1*10^5$ cells/cm² and the co-culture with a ratio of 90 %Caco-2 & 10% HT-29 at day 0. Leakage is given as the ratio of basal to apical fluorescence in percentage.

The most striking anomaly at first sight offers the data at day 5 post seeding, and is seen in all cell barriers. The randomness of the results indicate incorrect data. The possible sources of error could be due to wrong sample preparation or handling, although no deliberate modifications or alteration in the preparation of sodium fluorescein were made. The assumption that these

seemingly randomized values at day 5 are due to defect cell layers can be ruled out as the TEER at day 5 and 7 and the Na-flu leakage at day 7 show no abnormalities. Therefore, the results at day 5 are considered due to failure of procedure and are not considered significant. Further discussed results are related to the sodium fluorescein leakage at day 3 and 7.

For A549 cells the Na-flu leakage was reduced from 9.0 ± 5.6% at day 3 to 7.7 ± 2.2% at day 7 post seeding. A slightly higher reduction was achieved by the Caco-2 barrier from 12.0 ± 3.2% to 10.4 ± 2.2% and by the co-culture of Caco-2 & HT-29 from 9.3 ± 2.9% to 7.3 ± 3.4% of day 3 to day 7 post seeding, respectively. They are followed by an even higher leakage reduction for HT-29 cells from 9.8 ± 3.2% to 6.4 ± 4.0% and for BeWo b30 cells from 14.1 ± 3.3% to 9.2 ± 4.0% between day 3 and day 7 post seeding. The highest overall leakage showed the Hep G2 cell barrier with a Na-flu leakage of 17.6 ± 2.5% at day 3, which is comparatively high to the rest of the barriers, indicating that a less developed barrier was present that day. All the larger is the reduction to 6.1 ± 2.0% at day 7 post seeding.

The highest barrier tightness according to TEER values exhibit the co-culture of Caco-2 & HT-29 and Caco-2 cells. They also show the smallest reduction in Na-flu leakage over time. It can be a consequence of an early barrier tightness for these cell barriers. In contrast, the initial high sodium fluorescein leakage at day 3 and the strong reduction at day 7 for Hep G2 could be an indication that the cell line has a delayed barrier development compared to the other cell barriers. This assumption is supported by the reduced TEER value at day 3 for Hep G2 cells. Also, BeWo b30 cells start with a relatively high leakage at day 3 post seeding, followed with the second largest reduction after Hep G2 cells at day 7. This could be reason that BeWo b30 cells also form their tight barrier slightly delayed at the beginning, despite reading already high TEER values at day 3. Furthermore, HT-29 and A549 barriers are positioned in the intermediate area regarding Na-flu reduction from day 3 to 7 and absolute Na-flu leakage at day 7. The findings are reflected in the TEER readings, as both HT-29 and A549 also place themselves in the middle region in their TEER development. Other than that, the Na-flu results do not reflect the same assertions as found in TEER readings.

3.2. Barrier viability

In addition to monitoring parameters of barrier integrity, the viability information of these barriers was monitored using fluorescent dyes and the metabolic PrestoBlue™ assay. The viability was controlled in order to rule out influences of cell death on the integrity of the cell barrier on one hand and on the other hand to ensure an optimal precondition with healthy barriers for transport studies of glucose on day 7 and 8 post seeding. For the visual control, a live/dead staining with Calcein AM and Ethidium Homodimer-1 was performed at day 1, 3, 5, 7 and 8 post seeding. The metabolic assay with PrestoBlue™ was performed on the same days, whereby the results are given in percentage to the data of day 1. The findings are presented in Figure 3.3 for A549 cells, in Figure 3.4 for BeWo b30 cells, in Figure 3.5 for Caco-2 cells, in Figure 3.6 for HT-29 cells and in Figure 3.7 for Hep G2 cells. The highest metabolic activities was observed for Caco-2 cells with viability rates of 100 ± 3.1%, 127.6 ± 14.7%, 197.5 ± 20.8%, 248.4 ± 23.4%, 264.6 ± 14.5% for day 1, 3, 5, 7 and 8 post seeding, respectively. The results correlate well with the findings related to the barrier integrity. Lower, but still very high viability values could be recorded for BeWo b30 with 231.3 ± 3.7% and HT-29 with 204.5 ± 14.6% at day 8 post seeding. They are followed by A549 with 171.8 ± 6.4% and Hep G2 with 161.7 ± 3.5%. Same as in the parameters of barrier integrity, the viability rate of Hep G2 is the slowest in comparison, indicating of a slower proliferation rate in general.

The results of the metabolic activity based on PrestoBlue™ mirror the findings of the live/dead staining with CA AM and EthD-1. A confluent cell barrier was achieved for all cell types at day 3. Additional information from the vital dye staining is gained when examining the differences in the live/dead ratio of cells in the later days 7 and 8. At the early incubation days (day 3 and 5) all cell lines exhibit a predominant amount of viable (green) and an insignificant amount of non-viable (red) cells. As time progresses, differences in the quantity of dead cells between the cell lines BeWo b30 and A549 and the cell lines Caco-2 and HT-29 increase. The pictures suggest that A549 and BeWo b30 cells lack the ability to grow in a three dimensional fashion as the monitoring of their in the live/dead status reveals. The other cell lines are less affected by the long incubation and proliferation time as they grow in a three dimensional and non-damaging manner. This applies particular to the intestinal cell lines Caco-2 and HT-29, where the multilayers are apparent as surveys and valleys in Figure 3.5 and Figure 3.6 (a). This is also reflected in the smaller increase of viability for A549 and BeWo b30 in comparison to the other cell lines displaying a lower increase in metabolic activity of 4.9% and 4.7%, respectively. The cell line Hep G2 displays a moderate amount of cell death. They also show a low ability to grow multi-layered as small valleys are visible in the live staining with CA-AM staining at day 8.

Previous work observed the familiar ability to grow in multilayer fashion in Caco-2 cells (for late passage numbers) and HT-29 cells [100, 101]. Particularly in Caco-2 cells the transepithelial resistance increases for late passage numbers as they are more likely to grow multiple layers In contrast, the alveolar cancer cell line A549 grows as a 2D monolayer in in-vitro cell culture models. In long term cultivation, A549 cells differentiate towards alveolar epithelial type II [102]. Likewise, BeWo b30 mimics the placental barrier in a monolayer form in in-vitro. Even with increased initial seeding numbers, formation of multiple cell layers was not possible but only resulted in faster barrier confluence, which is the reason for this particular type of cell models being used frequently as in vitro model for placental trophoblasts [103].

The viability of the cell barriers is in particular important at day 7 and 8 in regard to the transport and inhibition studies of glucose. The findings indicate that the initial cell seeding density for A549 and BeWo b30 cells is too high for an incubation time of 8 days. For these cell lines a smaller seeding density or an overall smaller incubation and proliferation time could be considered for an optimal barrier. There are however no signs of barrier impairment present for these cell lines and necrotic cell just float above a tight and healthy cell barrier.

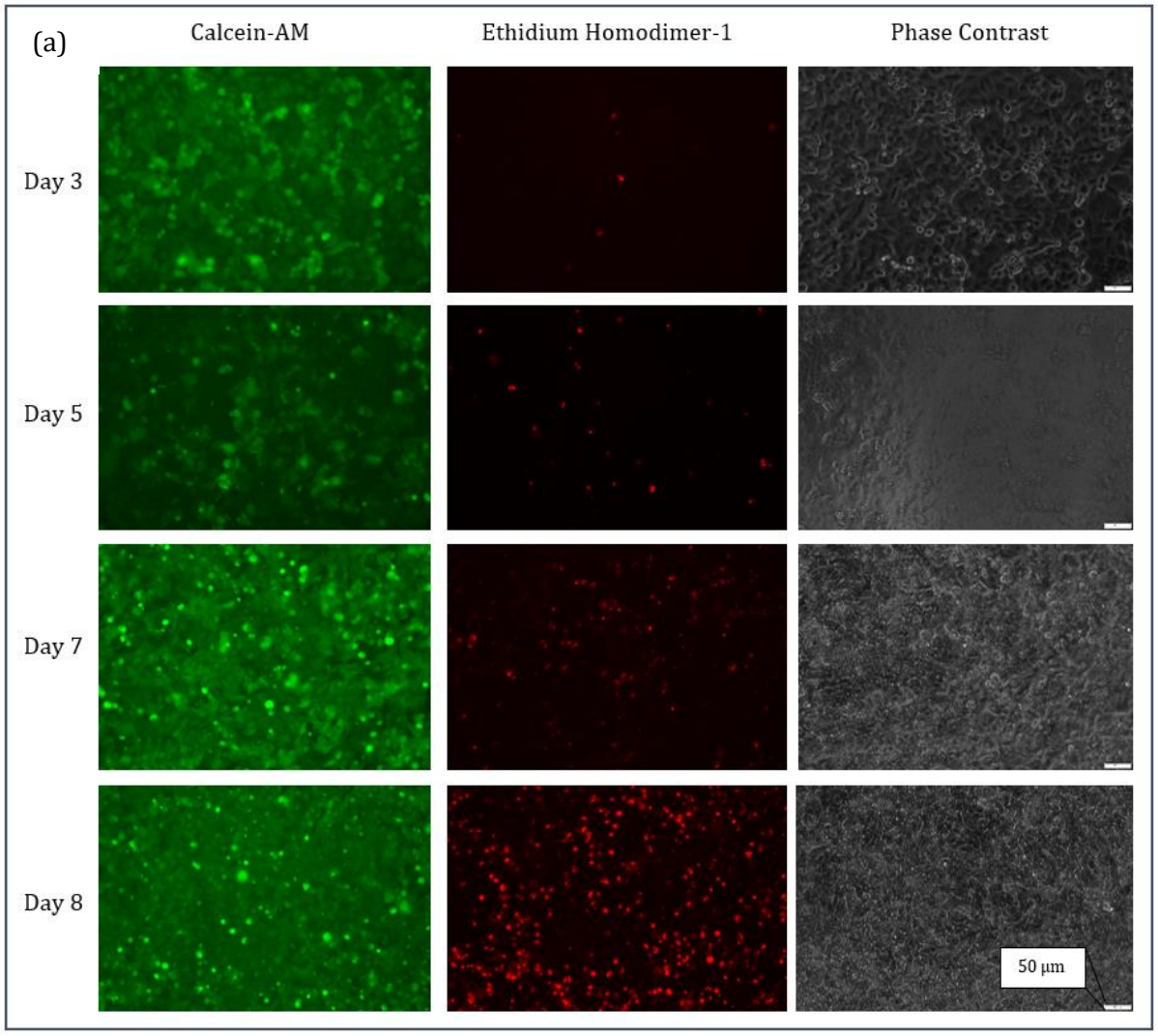

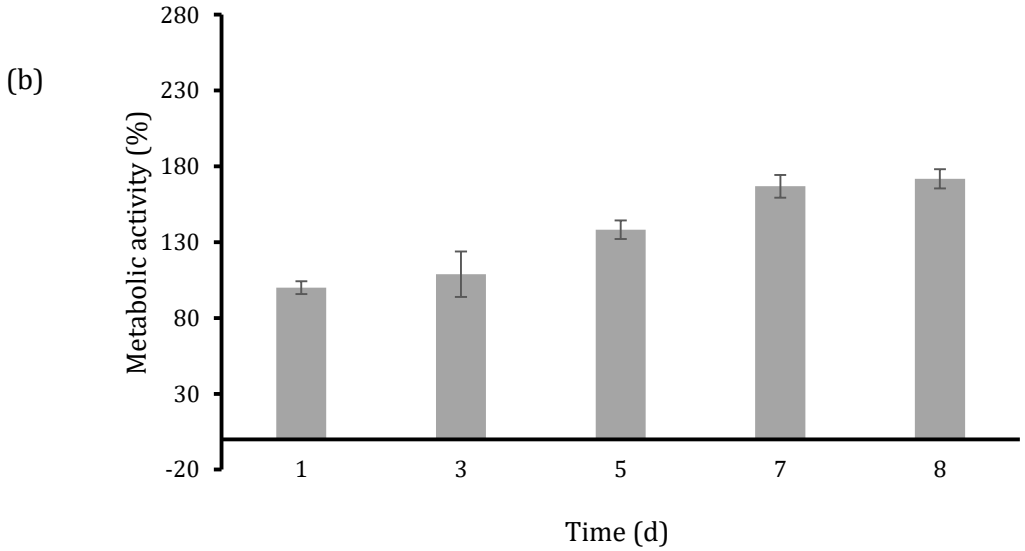

Figure 3.3: Evaluation of A549 viability/activity after 3, 5, 7 and 8 days in culture with: **(a)** Live-dead staining and phase contrast pictures. Calcein-AM for live (green) and Ethidium Homodimer-1 for dead (red) cells. Scale bar is 50 µm for all pictures. **(b)** PrestoBlue assay as an indicator for metabolic activity.

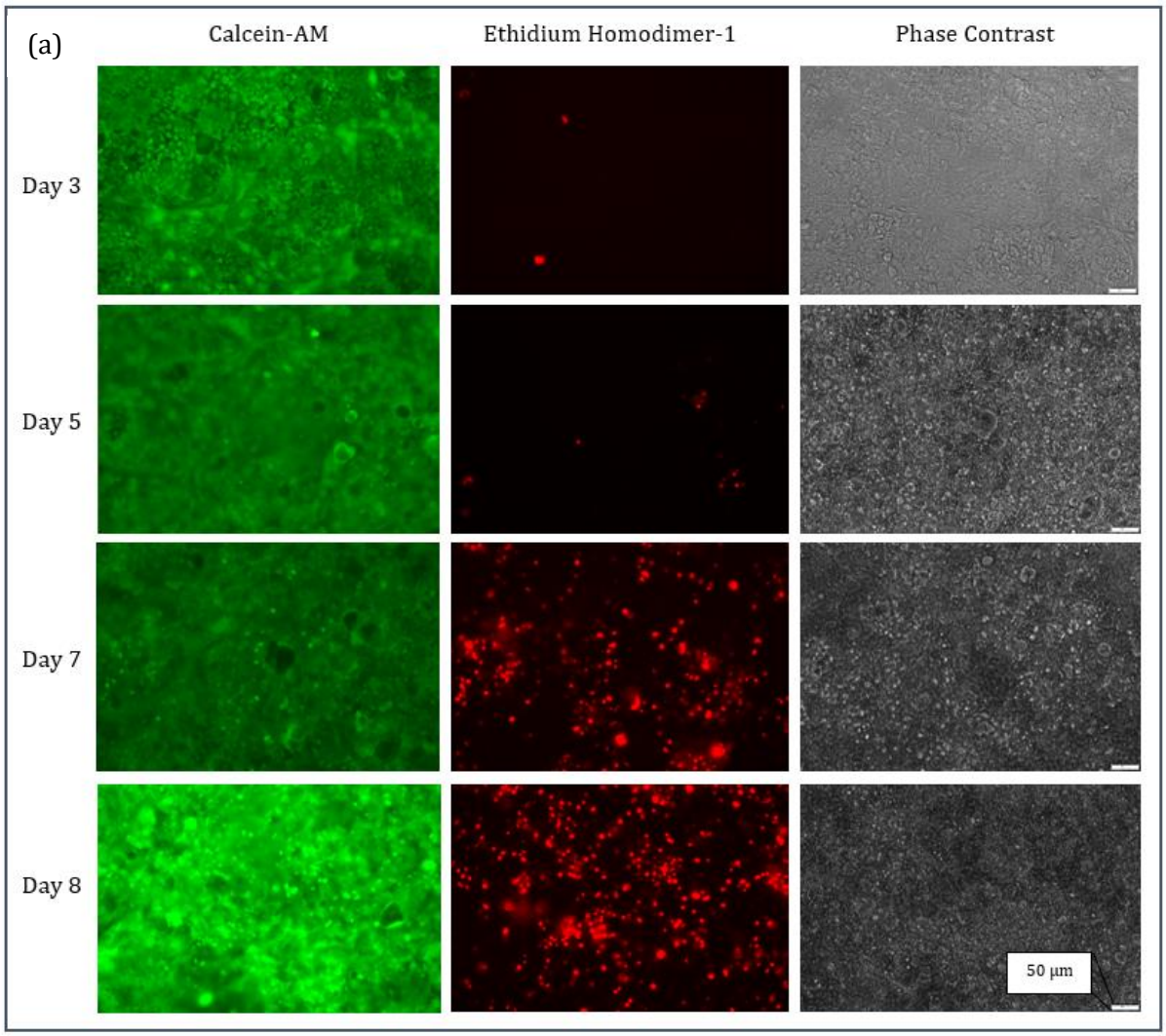

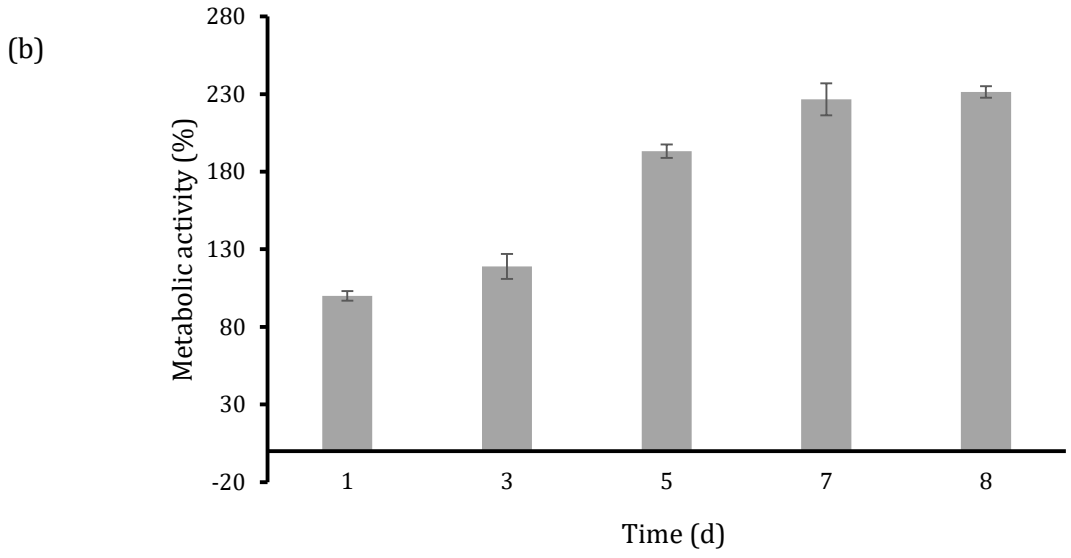

Figure 3.4: Evaluation of BeWo b30 viability/activity after 3, 5, 7 and 8 days in culture with: **(a)** Live-dead staining and phase contrast pictures. Calcein-AM for live (green) and Ethidium Homodimer-1 for dead (red) cells. Scale bar is 50 µm for all pictures. **(b)** PrestoBlue assay as an indicator for metabolic activity.

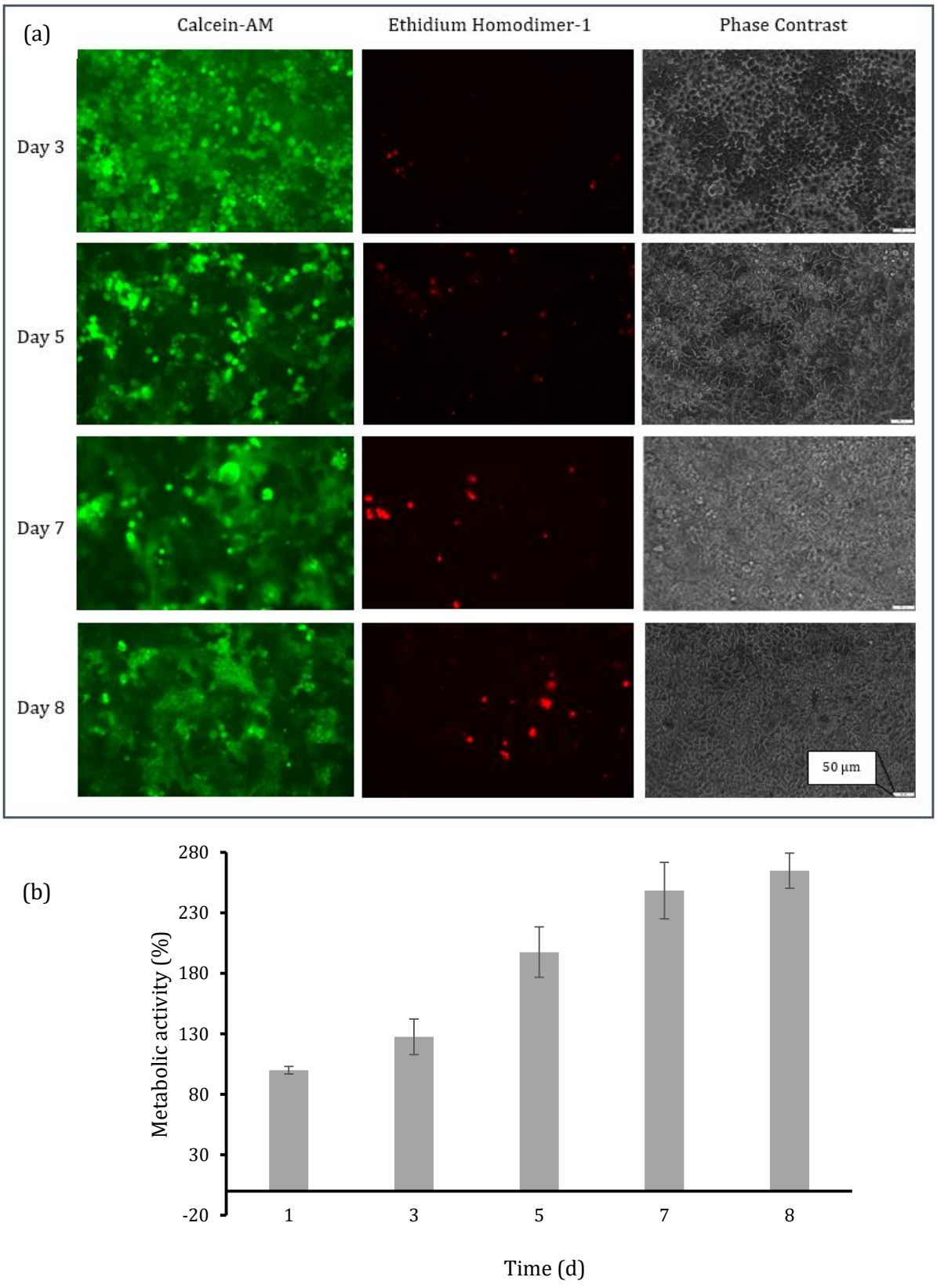

Figure 3.5: Evaluation of Caco-2 viability/activity after 3, 5, 7 and 8 days in culture with: **(a)** Live-dead staining and phase contrast pictures. Calcein-AM for live (green) and Ethidium Homodimer-1 for dead (red) cells. Scale bar is 50 µm for all pictures. **(b)** PrestoBlue assay as an indicator for metabolic activity.

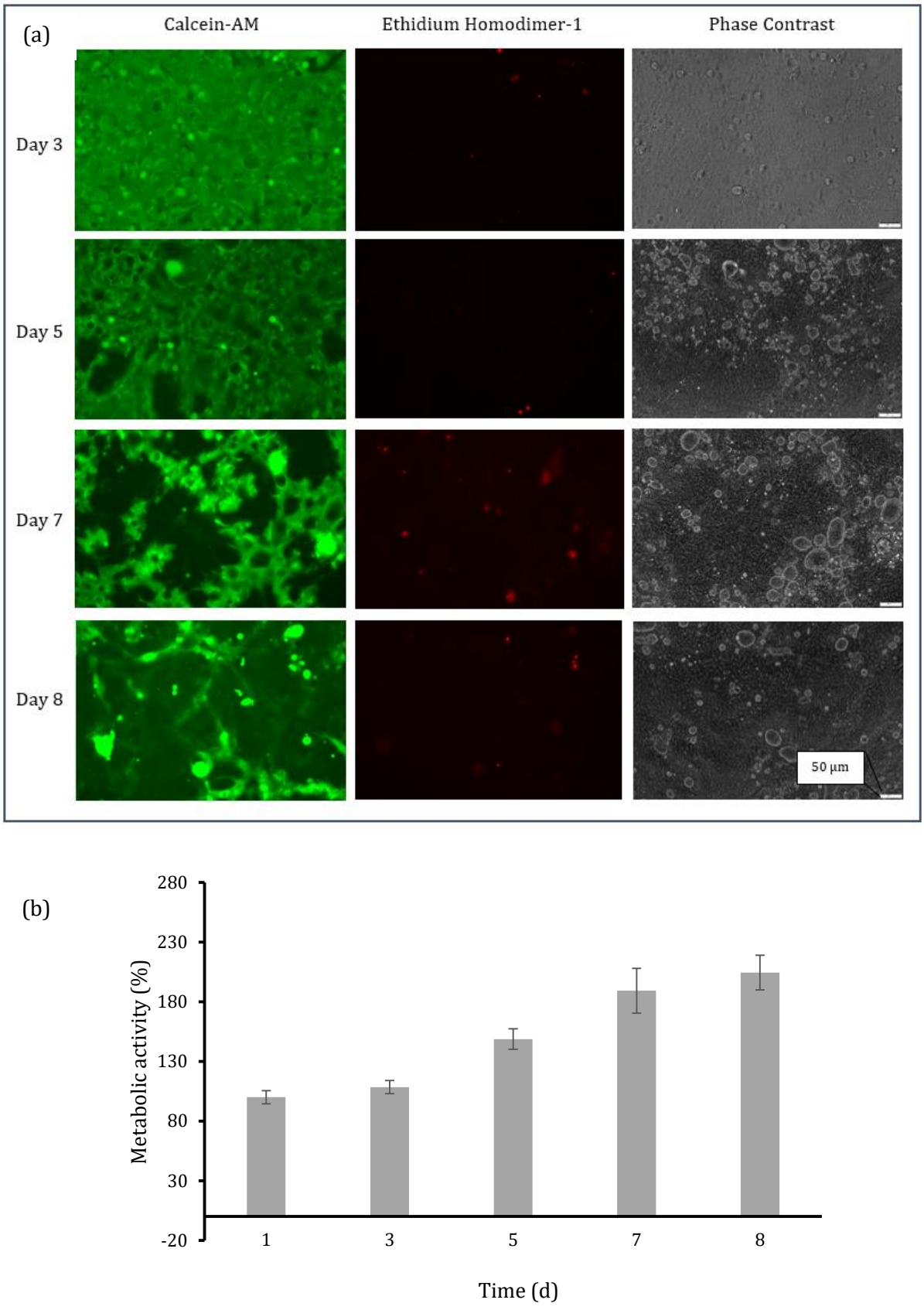

Figure 3.6: Evaluation of HT-29 viability/activity after 3, 5, 7 and 8 days in culture with: **(a)** Live-dead staining and phase contrast pictures. Calcein-AM for live (green) and Ethidium Homodimer-1 for dead (red) cells. Scale bar is 50 µm for all pictures. **(b)** PrestoBlue assay as an indicator for metabolic activity.

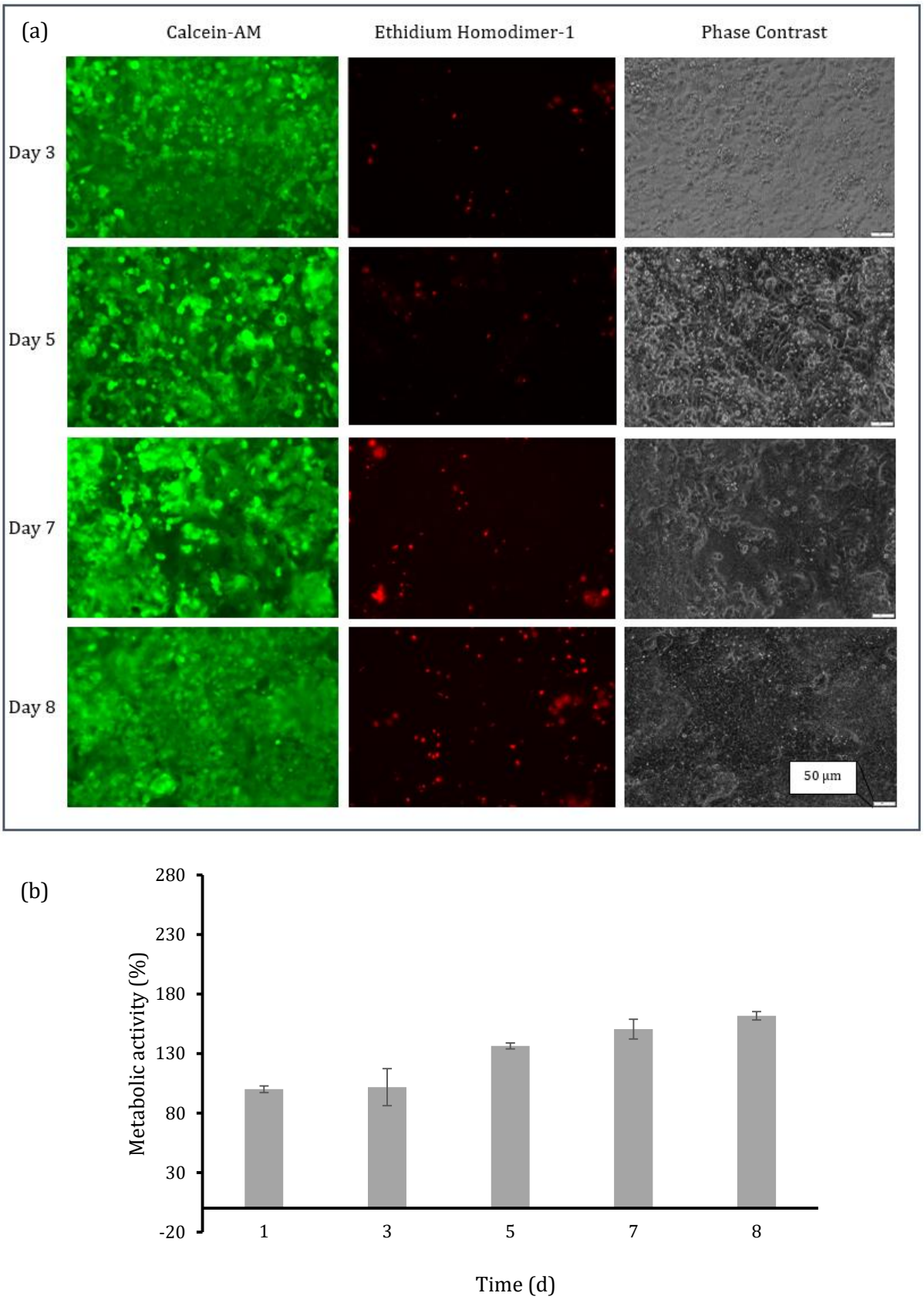

Figure 3.7: Evaluation of Hep G2 viability/activity after 3, 5, 7 and 8 days in culture with: **(a)** Live-dead staining and phase contrast pictures. Calcein-AM for live (green) and Ethidium Homodimer-1 for dead (red) cells. Scale bar is 50 µm for all pictures. **(b)** PrestoBlue assay as an indicator for metabolic activity.

3.3. Glucose transport processes of five human barriers

3.3.1. Calibration of IR spectroscopy and colorimetry for Glucose

Before any glucose concentration can be evaluated from absorbance data of the infrared spectrometer, a calibration of a prediction model must take place first. Figure 3.8 shows the smoothed and integrated absorbance spectra of $DMEM_{HIGH\ GLUCOSE}$, diluted with $DMEM_{NO\ GLUCOSE}$, in the range of 1180 cm^{-1} to 960 cm^{-1} as part of the first step in the prediction process. The solutions start with 4.5 mg/ml glucose and are diluted down to 0.125 mg/ml glucose.

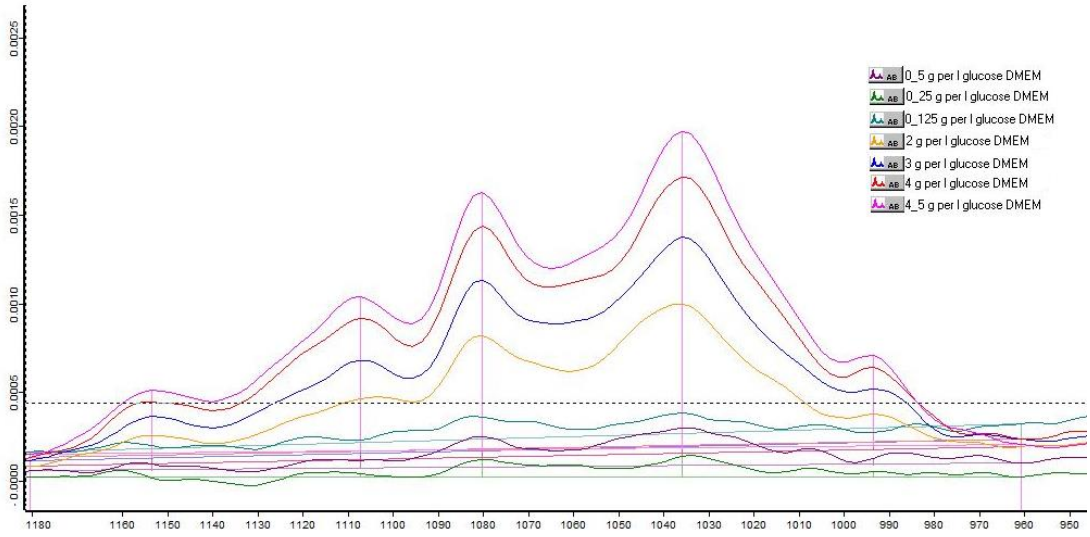

Figure 3.8: Glucose absorbance spectrum of the IR spectroscopy. The smoothed and integrated spectra is shown from 1180 cm^{-1} and 960 cm^{-1} for different glucose concentrations in DMEM solutions. The dilution series started with 4.5 mg/ml glucose $DMEM_{HIGH\ GLUCOSE}$ and was diluted with $DMEM_{NO\ GLUCOSE}$ down to 0.125 mg/ml glucose.

The spectrum shows typical local maxima of glucose due to the vibrational modes in the CO and CC stretching of the glucose molecule. The local maxima were determined at 1153.5 cm^{-1}, 1108 cm^{-1}, 1080.5 cm^{-1}, 1035.7 cm^{-1} and 994.3 cm^{-1} in accordance with the literature [93]. The absorbance values at the wavelength of 1035.7 cm^{-1} show the highest trend in absorption. This is due to strongest vibrational modes in the CO and vCC structure of glucose.

For the colorimetric detection of glucose a reference series starting from 4.5 mg/ml glucose down to 0.1 mg/ml glucose was diluted in a ratio of 1:130 to undermatch the maximum detectable limit

of the assay. Both, the absorbance data from IR spectroscopy of all local maxima and the fluorescence intensities of the colorimetric detection are plotted against the glucose concentrations in Figure 3.9. The corresponding linear regression analysis of the different IR wavenumbers and the fluorescence intensity, such as the regression coefficient R^2, LOQ and LOD are listed in Table 3.1 to find the best suited wavenumber for further analysis. The average RMS error of 2.0801* 10^{-5} of the IR spectrometer was measured from the wavenumbers 1200 to 990 cm^{-1}.

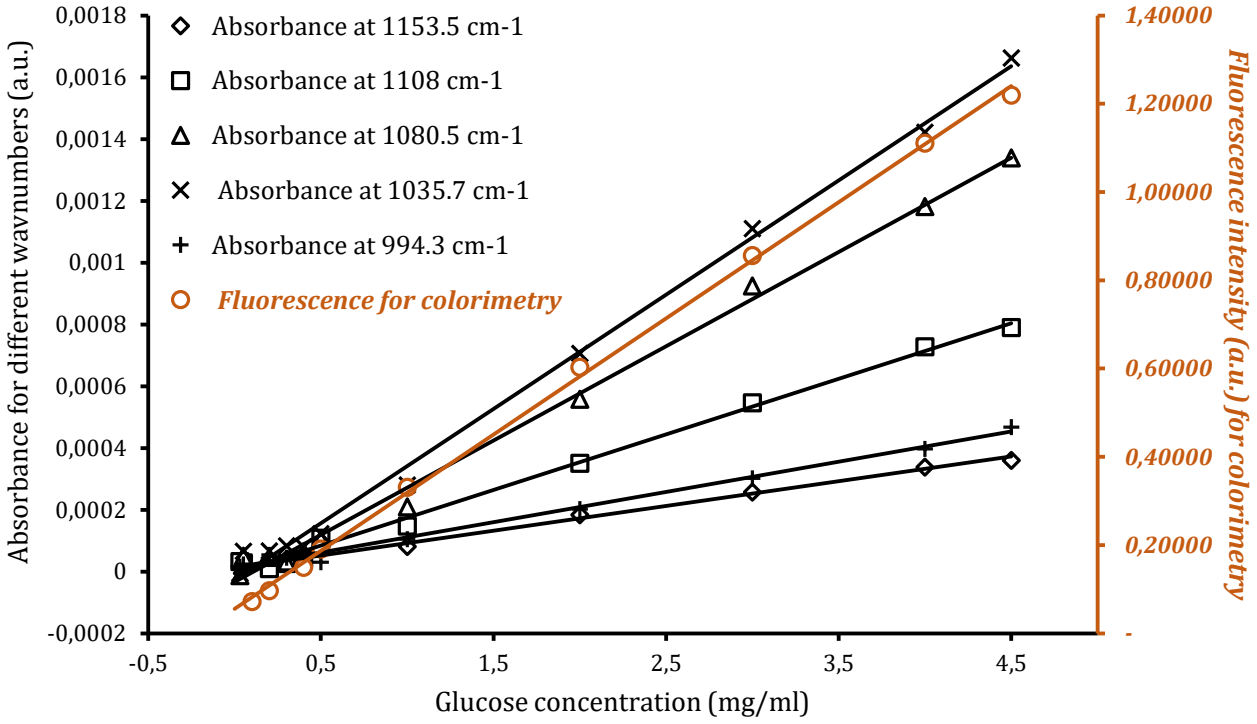

Figure 3.9: Comparison of absorbance data from IR spectroscopy for the wavenumbers 1153.5 cm^{-1}, 1108 cm^{-1}, 1080.5 cm^{-1}, 1035.7 cm^{-1} and 994.3 cm^{-1} (left y-axis) and fluorescence intensity of the enzymatic glucose assay (right y- axis) are plotted against the corresponding glucose concentrations. Linear regression line is included.

The limit of detection of the colorimetric approach amounts to 0.018 mg/ml glucose with a calculated regression coefficient R^2 of 99.6%. As seen in Figure 3.9, the calibration lines of the IR spectroscopy show the same linearity for corresponding glucose concentrations as for the colorimetric approach. Thus, it is justifiable to continue working with IR spectroscopy for the evaluation of future glucose measurements with the advantage of the benefits of a fast and label-free measurement method. The highest sensitivity for IR spectroscopy can be observed for absorbance values at the wavenumber 1035 cm^{-1}. For the wavenumber 1035 cm^{-1} the regression coefficient R^2 calculates to 99.6%, the smallest quantity of glucose which can be precisely detected is 0.169 mg/ml and the minimum amount of glucose which can be quantified is 0.564 mg/ml [95].

Table 3.1: List of regression analysis for glucose detection with IR spectroscopy for the wavenumbers 1153.5 cm^{-1}, 1108 cm^{-1}, 1080.5 cm^{-1}, 1035.7 cm^{-1} and 994.3 cm^{-1} and for enzyme based glucose detection assay. The averaged RMS error of the IR spectrometer is $2.0801 * 10^{-5}$, measured from the wavenumbers 1200 to 990 cm^{-1}.

		Linear Regression	R^2	LOD (mg/ml)	LOQ (mg/ml)
Wavenumber (cm^{-1})	1153.5	$y = 7.97*10^{-5} x + 1.33*10^{-5}$	0.989	0.783	2.611
	1108	$y = 1.80*10^{-4} x - 7{,}28*10^{-6}$	0.995	0.346	1.154
	1080.5	$y = 3.05*10^{-4} x - 3.27*10^{-5}$	0.995	0.205	0.683
	1035.7	$y = 3.69*10^{-4} x - 2.60*10^{-5}$	0.997	0.169	0.564
	994.3	$y = 9.64*10^{-5} x + 1.78*10^{-5}$	0.989	0.648	2.159
Colorimetric	Fluorescence intensity	y= 3.793 x + 0.055	0.996	$0.18*10^{-3}$	$0.60*10^{-3}$

The results show that the detection with IR spectroscopy at the wavenumber 1035.7 cm^{-1} behaves equally proportional to glucose concentrations as the colorimetric approach in the range between 0.01 and 4.5 mg/ml glucose. Therefore, the detection of glucose with the FTIR technique is a validate method to carry out glucose measurements. Therefore, all future calculations of glucose concentrations are conducted with IR spectroscopy at the wavenumber 1035.7 cm^{-1}, if not stated otherwise.

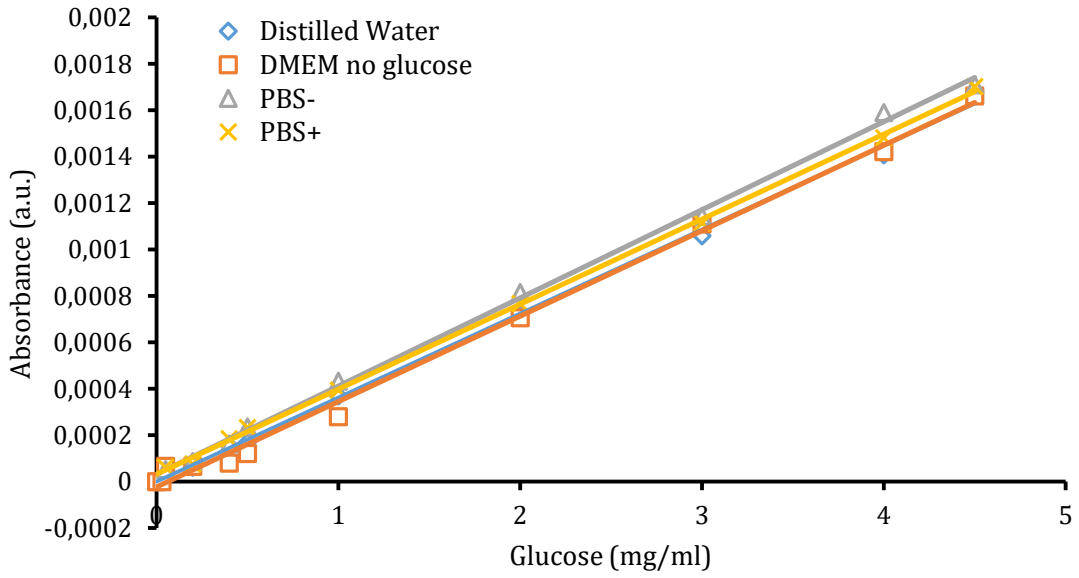

Figure 3.10: Absorbance data of IR spectroscopy is plotted against corresponding glucose concentrations at the wavenumber 1035.7 cm^{-1}. $DMEM_{HIGH\ GLUCOSE}$ was diluted with either $DMEM_{NO\ GLUCOSE}$, distilled water, PBS+ or PBS-. Linear regression line for each dilution series is included.

Cell culture media such as DMEM or Ham's F12 are not only liquids containing glucose, but also contain a high concentration of amino acids, vitamins and other supplements which are important

to sustain cell metabolism and promote proliferation. Therefore, in the next set of experiments, the influence of sample liquid composition on spectroscopy data was investigated to rule out any unwanted overlays of absorbance peaks at the most sensitive wavenumber towards glucose of 1035.7 cm^{-1}.

In order to investigate the influence of DMEM or PBS in the spectrum range of glucose, different dilution series of $DMEM_{HIGH\ GLUCOSE}$ with either $DMEM_{NO\ GLUCOSE}$, sterile distilled water, PBS- or PBS+ are shown in Figure 3.10. The graph evaluates the absorbance data at 1035.7 cm^{-1}. The according regression analysis is given in Table 3.2. The regression analysis confirms that the slopes of the linear fitting equations are very similar for all solutions used for the dilution. The measured absorbance values yield also high regression coefficients, where the highest of 99.9% is observed for the PBS solution.

Table 3.2: Regression analysis (R^2, LOD, and LOQ) of different dilution series. $DMEM_{HIGH\ GLUCOSE}$ was diluted with $DMEM_{NO\ GLUCOSE}$, distilled water, PBS+ or PBS- at the wavenumber, analysed with IR spectroscopy at the wavenumber 1035.7 cm^{-1}.

Dilution solution	Linear Regression	R^2	LOD (mg/ml)	LOQ (mg/ml)
$DMEM_{NO\ GLUCOSE}$	$y = 3.69*10^{-4}x - 2.60*10^{-5}$	0.997	0.168	0.561
Distilled water	$y = 3.62*10^{-4}x - 4.74*10^{-7}$	0.998	0.172	0.574
PBS+	$y = 3.17*10^{-4}x - 3.17*10^{-5}$	0.999	0.170	0.545
PBS-	$y = 3.80*10^{-4}x - 2.08*10^{-5}$	0.999	0.164	0.568

In the work of Sulé-Suso et al. [104], the addition of $CaCl_2$ and $MgCl_2$ on lung cancer cells caused a relocation of maxima between 3290 and 3395 cm^{-1} and from 1631 cm^{-1} downwards respectively. There was also an increase at 1410 cm^{-1} in the FTIR spectrum. They observed no apparent effects in the spectrum between the wavenumbers 1153.5 - 994.3 cm^{-1} for containing $CaCl_2$ and $MgCl_2$. The results are in accordance with the published word of Sulé-Suso et al. However, a small positive offset for graphs with PBS compared to DMEM is noticeable in Figure 3.10 which can be attributed to a negligible offset due to phosphate in the buffer.

3.3.2. Characterisation of transport processes

For the characterisation of the glucose transport processes, glucose concentrations during the apical-to-basal transport of the transwell experiment were analysed for each cell barrier, co-culture and acellular control.

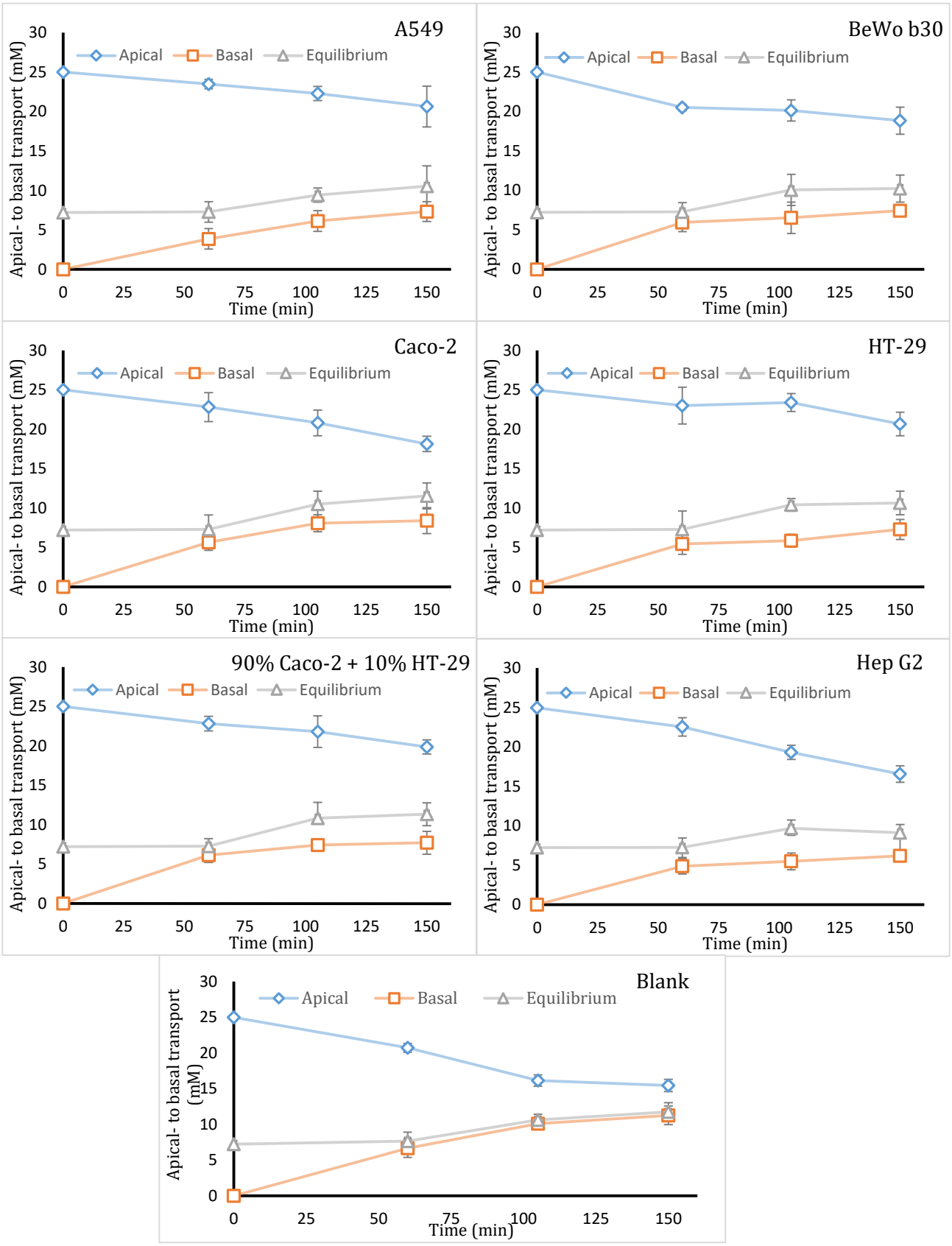

Figure 3.11: Time course of apical and basal glucose transport for all barriers and acellular control at day 7 post seeding. Glucose concentration was analysed with IR spectroscopy at 1035.7 cm^{-1}. Apical glucose concentration in blue, basal glucose concentration in orange and calculated volume corrected state of equilibrium in grey.

The cells were seeded at a density of 1* 10^5 cells per transwell and the experiment was performed at day 7 post seeding with confluent cell barriers. The integrity of the barriers were assessed with TEER and sodium fluorescein leakage assay. The courses of TEER and Na-flu reduction for each barrier are discussed in Chapter 3.1.1 and 3.1.2. Samples of apical and basal chambers were taken after 0, 60, 105 and 150 minutes and kept at – 20°C prior to FTIR analysis.

Figure 3.11 shows the time course of glucose concentrations in apical and basal chambers, evaluated at the most sensitive of wavenumber of 1035.7 cm^{-1}. The dotted line shows an approximation of the equilibrium of apical and basal glucose concentration. The approximations are corrected for the volume loss of 50 µl at each time point. For better recognition on how fast the barriers reach the equilibrium, Figure 3.12 shows the relation of basal to apical glucose concentration as a function of time. The concentration in the apical and basal chamber is referred to as c_A and c_B, respectively. An equilibrium of glucose concentration is reached when apical and basal glucose concentration is equal, which is the case for a ratio of 1 in Figure 3.12. As expected, the fastest development towards equilibrium can be seen in the no-cell control with 73 ± 4% after 150 minutes. In contrast, cell barrier models showed decreasing glucose transport rates of 46 ± 3% for Caco-2, 40 ± 4% for BeWo b30, 39 ± 3% for the co-culture of Caco-2 and HT-29, Hep G2 cells with 37 ± 3%, A549 with 35.6 ± 2.8% followed by HT-29 with the lowest glucose transport of 35 ± 3% after 150 minutes.

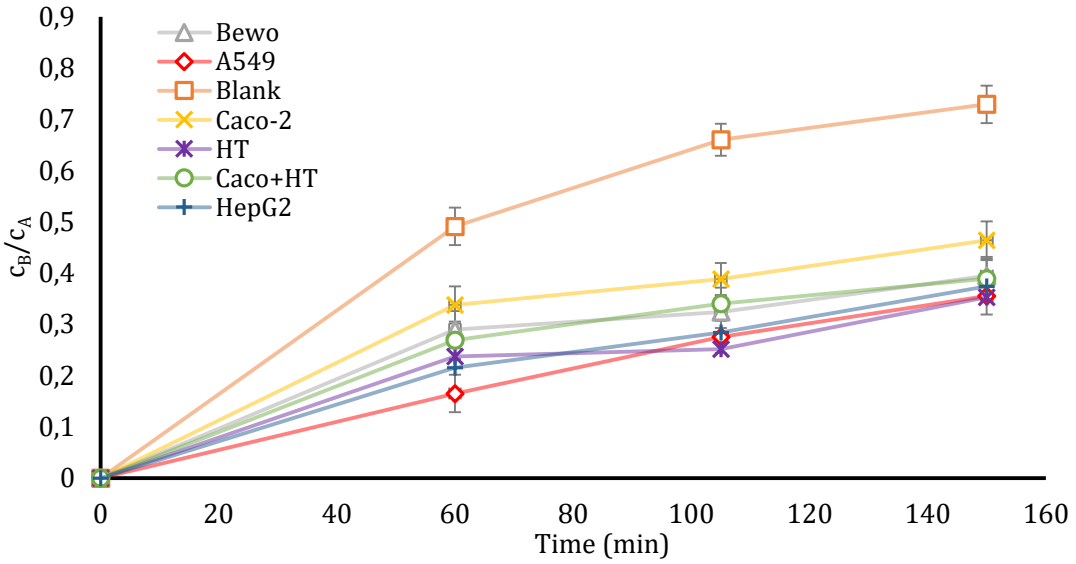

Figure 3.12: Time course of the ratio of basal glucose concentration (c_B) to apical glucose concentration (c_A) of all cellular barriers and acellular control to reach equilibrium (≙ 100%) at day 7 post seeding. Glucose concentrations were measured with IR spectroscopy, evaluated at the wavenumber 1035.7 cm^{-1}.

The results of the transport rate is based on the transfer of basal glucose concentrations. Similar to the illustration of the ratio of c_B/c_A, the transport rates reveal comparable information about the glucose transport capability of the presented human cell barriers. The glucose transfer rates

are high at the beginning of the transport process followed by a decrease over time. The fastest glucose transport is obviously detected in the acellular control due to glucose diffusion processes with 6.7 ± 0.3 mM/h at 60 minutes, 4.6 ± 0.2 mM/h at 105 minutes and 1.6 ± 0.2 mM/h at 150 minutes.

At 60 minutes the highest cellular transfer rates can be found for the co-culture of Caco-2 & HT-29 with 6.1 ± 0.3 mM/h, followed by BeWo b30 with 5.9 ± 0.2 mM/h, Caco-2 with 5.7 ± 0.2 mM/h, HT-29 with 5.5 ± 0.3 mM/h, Hep G2 with 4.9 ± 0.2 mM/h and finally A549 with 3.9 ± 0.2 mM/h. For a complete list of the transport rates in mM/h at 60, 105 and 150 minutes, Table 3.3 provides the results for all barriers and the no-cell control.

Overall, the intestinal barriers Caco-2 and co-culture of Caco-2 with HT-29 display the fastest glucose transfer barriers. The high glucose transfer rates of the intestinal cells is not surprising, since one of their primary tasks is to facilitate the transfer of glucose from the intestinal lumen to the blood [105]. Also the placental barrier BeWo b30 exhibits high transfer rates, and overshadow the rates of the lung and the hepatic barriers, which also makes sense due to the fact that placental glucose transport is critical to sustain fetal development and health throughout gestation [106].

Table 3.3: List of transport rates of all barriers and no-cell control after 60, 105 and 150 minutes. Transport rate is given in mM/h and is based on the transfer of basal glucose. Glucose concentrations were measured with IR spectroscopy, evaluated at the wavenumber 1035.7 cm^{-1} at day 7 post seeding.

	Transport rate (mM/h) at		
Barrier	60 min	105 min	150 min
Blank	6.7 ± 0.3	4.6 ± 0.2	1.6 ± 0. 2
A549	3.9 ± 0.2	3.0 ± 0.2	1.6 ± 0.2
BeWo b30	5.9 ± 0.2	0.8 ± 0.4	1.2 ± 0.3
Caco-2	5.7 ± 0.2	3.2 ± 0. 3	0.3 ± 0.4
HT-29	5.5 ± 0.3	0.6 ± 0. 2	1.9 ± 0.3
Caco-2 & HT-29	6.1 ± 0.3	1.7 ± 0. 3	0.4 ± 0. 2
Hep G2	4.9 ± 0.2	0.8 ± 0. 2	1.0 ± 0.3

The aim of the analysis of glucose transport in different barriers process was to study the transport processes of the individual cell barriers and to find suitable time points for the further investigation of glucose transport with inhibitors. The lowest measured concentration of glucose was 0.698 mg/ml after 60 minutes transport time at the basal side of the A549 barrier. The limit of detection of IR spectroscopy measured 0.169 mg/ml at the wavenumber 1035.7 cm^{-1} and therefore fulfils the requirements for adequate glucose detection with IR spectroscopy. In the further course, the transport times of 60 and 120 min were selected to execute the inhibition experiments.

3.4. Glucose transport inhibition with cytochalasin B and phloretin

To gain a better understanding of the cell surface distribution and activity of various types of glucose transporters, next the effect of glucose transport inhibitors was investigated. The results show the comparative glucose transport inhibition of five human in-vitro barriers with three different commonly used glucose transporter inhibitors. The individual inhibitors were added at day 7 post seeding and incubated for 24 hours. Previously, the barrier integrity was assessed with TEER at day 7 and showed normal readings for each barrier. Glucose transport measurements were conducted at day 8 post seeding. The glucose concentrations were analysed with vibrational IR spectroscopy. A complete table of glucose transport inhibition for all barriers in relation to their no-treated cell control can be found in Table 3.4.

Results of glucose transport inhibition with 20 µM cytochalasin B are shown in Figure 3.13. The glucose transport was measured after 60 minutes. The list of transporters above each cell line is shown to indicate the frequency of GLUT and SGLT transporters expressed by each of the barrier models with the exception of A549 (the rank of transporters is not known to date). Highlighted transporters in blue colour are subject to inhibition, whereas black coloured transporters are present, but not subject of inhibition. The glucose transport of CB treated cells is given in relation to the transport of the corresponding non-treated cell barriers. For BeWo b30 an inhibition of 53 ± 11% relative to non-treated BeWo b30 cells was observed. A reduction in transport of 42 ± 13% was determined for the CB treated Hep G2 barrier cells. A549 cells showed a transport decline of 35 ± 13% with CB treatment. For the barriers of Caco-2, Caco-2 & HT-29 co-culture and HT-29 the transport was inhibited by 19 ± 8%, 12 ± 6% and 16 ± 7%, respectively. The highest reduction of passive glucose transport was found for the BeWo b30 and Hep G2 cell barrier. BeWo b30 cells are trophoblast cells derived from the first trimester of the pregnancy, where GLUT3 is highly expressed in the placental tissue [34]. Therefore both, GLUT1 and GLUT3 are important transporters in BeWo b30 cells. GLUT1 is in general extremely over expressed in the cancer lines A549, BeWo b30, Caco-2, HT-29 and Hep G2 as mentioned earlier [40]. The high inhibition rate in BeWo b30 could originate from the ability of GLUT1 and GLUT3 to be blocked by cytochalasin B [30, 72]. Additionally, GLUT9, 10, 12 are transporters found in the placenta, but in unknown concentrations. Of those, only GLUT10 can be inhibited by CB. GLUT12 is expressed in the first trimester but its affinity to glucose is not known [27, 30, 34]. Therefore, the reduction of over 50% of glucose transport due to CB can be attributed to a high occupancy of GLUT1, GLUT3 and/or GLUT 10 transporters on the cell membrane of BeWo b30 cells.

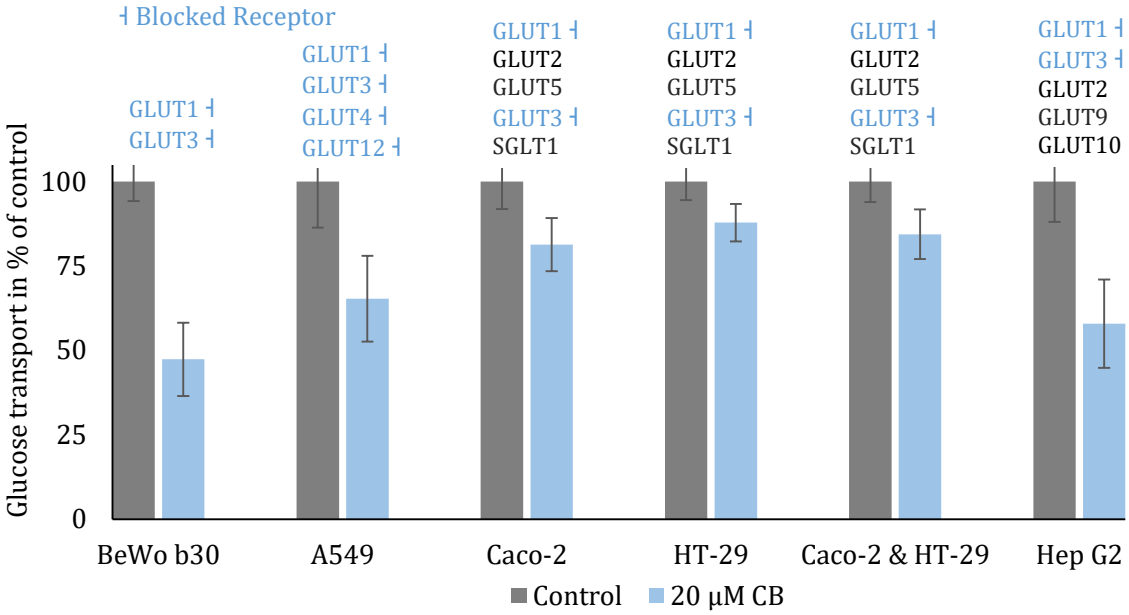

Figure 3.13: Results of glucose transport of all barriers after treatment with 20 µM cytochalasin B at day 7 post seeding for 24 hours. Transport of glucose was measured after 60 minutes at day 8 with IR spectroscopy at the wavenumber 1035.7 cm^{-1}. Transport rate is given in percentage to each cell control without treatment with CB. All GLUTs expressed in the according cell line are ranked by the amount of expression above, except for A549. Colour-coded (┤) GLUTs are subject to inhibition by CB.

Similar to BeWo b30, the dominating transporters in Hep G2 cells are GLUT1 and GLUT3, both inhabitable by CB. There are however other transporters such as GLUT2, 9 and 10 expressed in Hep G2 of which none show affinities to CB [58], indicating that these transporters are likely to account for around 60% of glucose transporters on this hepatic cell line.

For lung there is unfortunately not much known to date about the amount of GLUT1, 3, 4 and 12 expression in A549 cells or if any other types are present. In contrast, GLUT1, 2 and 8-10 are expressed in human lung tissue, where GLUT1 and GLUT2 are responsible for the basal glucose release [12, 27]. Even though all of the GLUTs known for A549 cells can be subject to inhibition by CB, relatively mediocre inhibition of glucose transport of around 35% was observed for CB treated samples.

The results for the intestinal barriers demonstrate generally lower transport inhibition for Caco-2, HT-29 and/or their co-culture. This is most due to the fact that Caco-2 and HT-29 are the only barriers with receptors for SGLT1. As mentioned SGLT1 is an active transporter of glucose and not influenced by cytochalasin B. Additionally, with respect to the other GLUTs present in the intestinal barrier only GLUT1 is binding to CB suggesting that the lower inhibition in these barriers can be attributed to the significantly much higher expression of SGLT1 as well as the presence of mostly GLUTs that are not blocked by CB.

The results of glucose transport inhibition with 30 µM phloretin (PT) are shown in Figure 3.14. The transport of glucose was measured after 120 minutes in PT treated and non-treated cell barriers. Likewise to the inhibition of CB, the transport is given in relation to non- treated cells. At first sight it seems that phloretin is capable of binding to most GLUTs expressed in the cancer cells lines with the exceptions GLUT5, GLUT9 and GLUT12. However, transport of GLUT5 is specific for fructose and GLUT9 is a transporter for urate [27, 42]. Regardless, lower inhibition rates of 20 ± 4% for A549 and 38 ± 12% for BeWo b30 are measured compared to with CB. The calculated inhibition value of 36 ± 9% for Hep G2 is slightly lower for phloretin than for CB. In contrast, higher inhibition rates for the intestinal barriers Caco-2 with 45 ± 16%, HT-29 with 24 ± 12% and co-culture Caco-2 & HT-29 with 27 ± 8% were achieved.

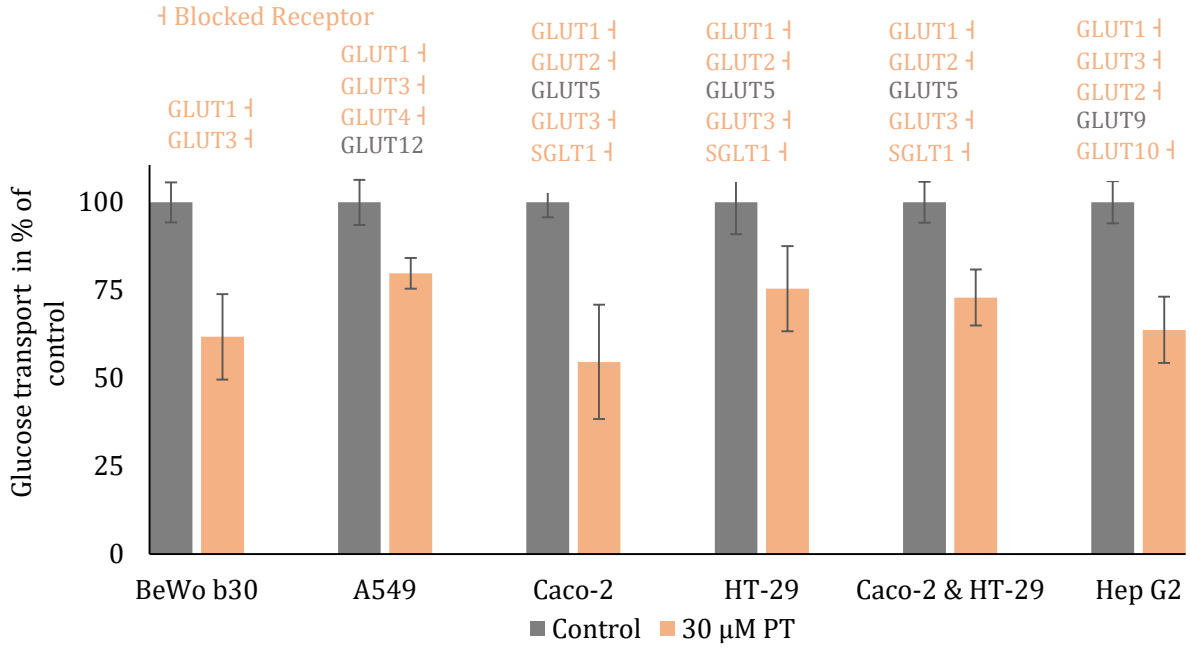

Figure 3.14: Results of glucose transport of all barriers after treatment with 30 µM phloretin at day 7 post seeding for 24 hours. Transport of glucose was measured after 120 minutes at day 8 with IR spectroscopy at the wavenumber 1035.7 cm^{-1}. Transport rate is given in percentage to each cell control without treatment with PT. All GLUTs expressed in the according cell line are ranked by the amount of expression above, except for A549. Colour-coded (┤) GLUTs are subject to inhibition by PT.

Phloretin blocks the transporter GLUT1, 3 and 4 in A549 cells. But when comparing the affinities of cytochalasin B and phloretin to GLUT1 and GLUT4, differences can be detected. The half maximal inhibitory concentration, IC_{50}, for GLUT1 is lower for CB than for phloretin. In GLUT1 it measures an IC_{50} of 0.44 µM for cytochalasin B and an IC_{50} of 49 µM for phloretin [32]. Similar conditions are found for GLUT4, where it is inhibited with an IC_{50} of 0.2 µM by CB and an IC_{50} of 10 µM by PT [74]. So even if CB and PT are both inhibitors of GLUT1 and GLUT4, CB has a stronger inhibitory effect. Additionally, GLUT12, which is expressed in A549 cells, is not inhibited by

phloretin. Considering all these facts, the weaker inhibitory strength of phloretin in A549 seems logical.

In Hep G2 the inhibition of GLUTs with PT produces similar results to CB, although GLUT2 and GLUT10 are additionally blocked with PT. But as mentioned before, the transport of glucose in Hep G2 cells is proposed to be mainly due to the high expression of GLUT1 and GLUT3, where the inhibitory impact of phloretin is smaller compared to cytochalasin B. Similar to Hep G2, the lower inhibition of glucose transport in BeWo b30 is suggested due to the lower strength of phloretin inhibition of GLUT1.

However, in the case of the intestinal barriers Caco-2, HT-29 and their co-culture the distribution of inhibition shifts towards high inhibition rates for phloretin. In contrast to Hep G2 cells, GLUT2 plays a far more important role in both intestinal barriers [63]. In addition, Caco-2 and HT-29 both express receptors of the active glucose transporter SGLT1 [66]. Even with the small affinity of phloretin to SGLT1 (Ki = 50 µM [78]), together with the inhibition of GLUT1 and GLUT2 [69, 76], a significant reduction of glucose transport in these barriers was achieved. However, the strength of inhibition in Caco-2 is higher than for its intestinal relative HT-29 or their co-culture.

3.5. Effect of cell apoptosis and necrosis on glucose transport and IR spectrum

A valuable attribute of IR spectroscopy is that it returns knowledge of all molecules in a solution. Therefore, IR spectroscopy can also be used as an analysis tool for cellular processes such as conformational alterations in cells or apoptosis initiated by chemical compounds [107]. In general, apoptosis is the programmed cell death and can initiate deterioration or inflammation reactions. In cell culture it can be triggered when exposing the cells to different agents, high temperature, or through withdrawal of vital nutrients. Apoptotic cells experience transformation changes in their charges, changes in permeability or proteins in their cell membranes [108].

In order to investigate the effect high phloretin concentrations on the cell barriers, the glucose transport experiment was repeated with 1 mM instead of 30 µM phloretin. It was predicted, that in high dosages above 0.1 mM phloretin the cytotoxic effect of phloretin predominates and that viability rates in the A549 cell line decrease down to 50 % [109]. The glucose transport of treated cells would align with transport characteristics of simple diffusion processes of glucose as cell apoptosis would increase and cell-to-cell networks of the barriers would break.

The results identified differences in the IR spectrum with 1 mM PT particularly at wavenumbers from 990 cm^{-1} and 1240 cm^{-1} and from 2680 cm^{-1} to 2960 cm^{-1}. Since these effects were not observed for lower concentrations of phloretin or cytochalasin B, the differences in both spectra are not attributed to the compound phloretin.

In the work of Gaudenzi et al. [107], several markers in IR spectroscopy were connected to cell apoptosis. In spectrum of glucose, asymmetric stretching of nucleic acid and DNA were detected at 1235 cm^{-1}, CO stretching of nucleic acid sugar and COP stretching of lipids at 1084 cm^{-1}. Nucleic acid ribose produces CO vibrations at the wavenumber 1056 cm^{-1}. Further, asymmetric stretches of CH_3 and CH_2 at the wavenumbers 2960 cm^{-1} and 2928 cm^{-1} were detected. The interferences also cover the detection range of glucose and are suggested to arise from the high number of cell deaths, causing signals of nucleic acid sugars at the same wavenumbers. This in turn challenges the ability to precisely detect glucose transport with certainty. These interferences were also noticed in the IR spectrum of the PT treated cell barriers.

Summarised, cell apoptosis induced by chemical agents such as phloretin, causes CO stretching of nucleic acid sugars and COP stretching of lipids to overlap the infrared spectrum of glucose, which is originally caused by CC and CO vibrations. The results show, that the possibility of detecting glucose during glucose movement through apoptotic cells is hardly possible.

In order to investigate the effect of WZB-117, an effective anti-cancer drug, on IR glucose spectrum and glucose transport of the cell barriers, transport measurements were performed after treatment with 20 µM WZB-117 for 24 hours.

The results of glucose transport of the barriers after is shown in Figure 3.15. The IC_{50} value of WZB-117 amounts to 10 µM [110]. Interferences in the IR spectrum were detected for A549 and BeWo b30 cells at the wavenumber range of glucose, where the only wavenumber not affected was at 1153.5 cm^{-1}. Therefore, the transport was evaluated at the wavenumber 1153.5 cm^{-1} for the analysis of transport inhibition for A549 and BeWo b30. An excerpt of the interferences in A549 cells is shown in Figure 3.16 and discussed below. An inhibition of 8 ± 9% was measured for A459 cell barrier and a reduction of 9 ± 8% was examined in BeWo b30. Transport decline of 13 ± 8% was determined in Caco-2 cell barrier, 8 ± 7 in the Caco-2 & HT-29 co-culture and 16 ± 9% in the HT-29 barrier.

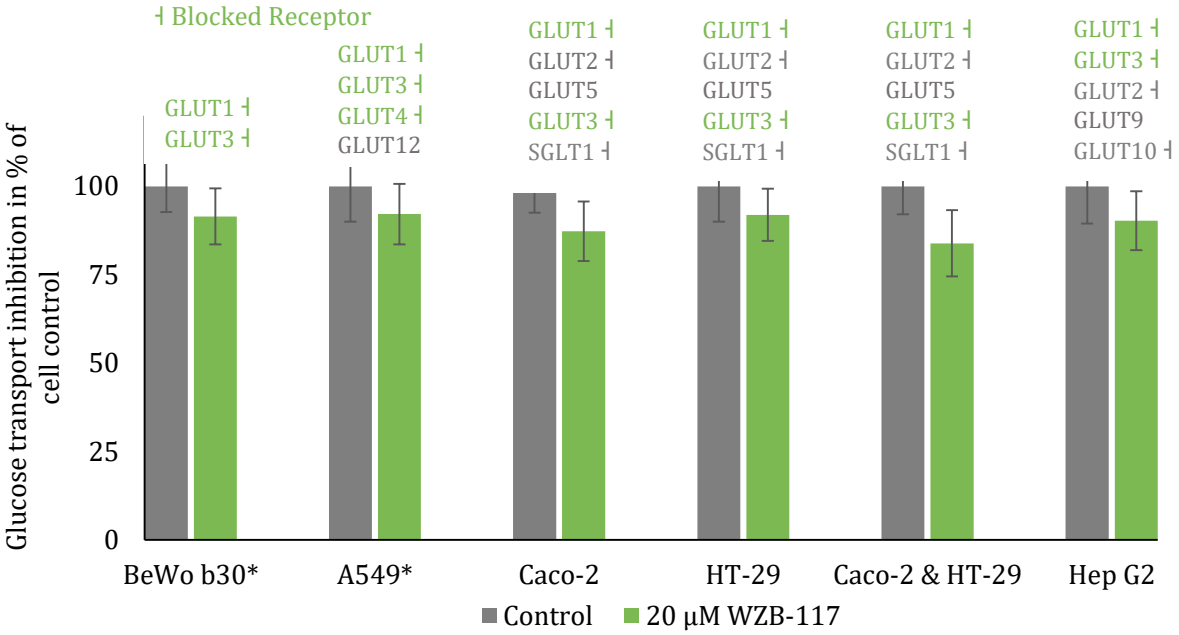

Figure 3.15: Results of glucose transport of all barriers after treatment with 20 µM WZB-117 at day 7 post seeding for 24 hours. Transport of glucose was measured after 120 minutes at day 8 with IR spectroscopy at the wavenumber 1035.7 cm^{-1}, (*) marked cell barriers at the wavenumber 1153.5 cm^{-1}. Transport rate is given in percentage to each cell control without treatment with WZB-117. All GLUTs expressed in the according cell line are ranked by the amount of expression above, except for A549. Colour-coded (⊣) GLUTs are subject to inhibition by WZB-117.

WZB-117 inhibits the passive transport with GLUT1, 3 and 4, restricts glycolysis and constrains the development of cancer. The inhibition of GLUT4 is higher than of GLUT1 and GLUT3 [68]. Studies suggest, that even small concentrations of WZB-117 have cytotoxic effects on cancer cell lines, where A549 cells treated with 10 µM WZB-117 experienced senescence and necrosis after 24 hours. WZB-117 is the first GLUT1 inhibitor which induces necrosis rather than apoptosis. The

difference of necrosis to apoptosis is that ATP is used during apoptosis. It was concluded that WZB-117 reduces ATP in the cells making them incapable of apoptosis [110].

An excerpt of the interferences during A549 cell transport studies in the IR spectrum of glucose is shown in Figure 3.16. For comparison, the spectrum of $DMEM_{HIGH\ GLUCOSE}$ is shown. The interferences occur between the wavenumber 990 cm^{-1} and 1140 cm^{-1}. However, the eigenfrequencies of glucose at the wavenumbers 1153.5 cm^{-1} and 994.3 cm^{-1} are not significantly impaired by the overlays. The negative interferences in WZB-117 treated A549 and BeWo b30 cells are not similar to the interferences induced by apoptosis due to the cytotoxic effects of 1 mM phloretin. They do occur at the regions of glucose vibrations, but primarily differ in their polarity. It is not clear if the inhibition detected reflect the amount of inhibition of GLUT1, 3 and 4 in the cell barriers, or if they are partially impaired by the anti-cancer effect of WZB-117 or other causes which responsible for negative interferences. Transport inhibition was still evaluated for A549 and BeWo b30.

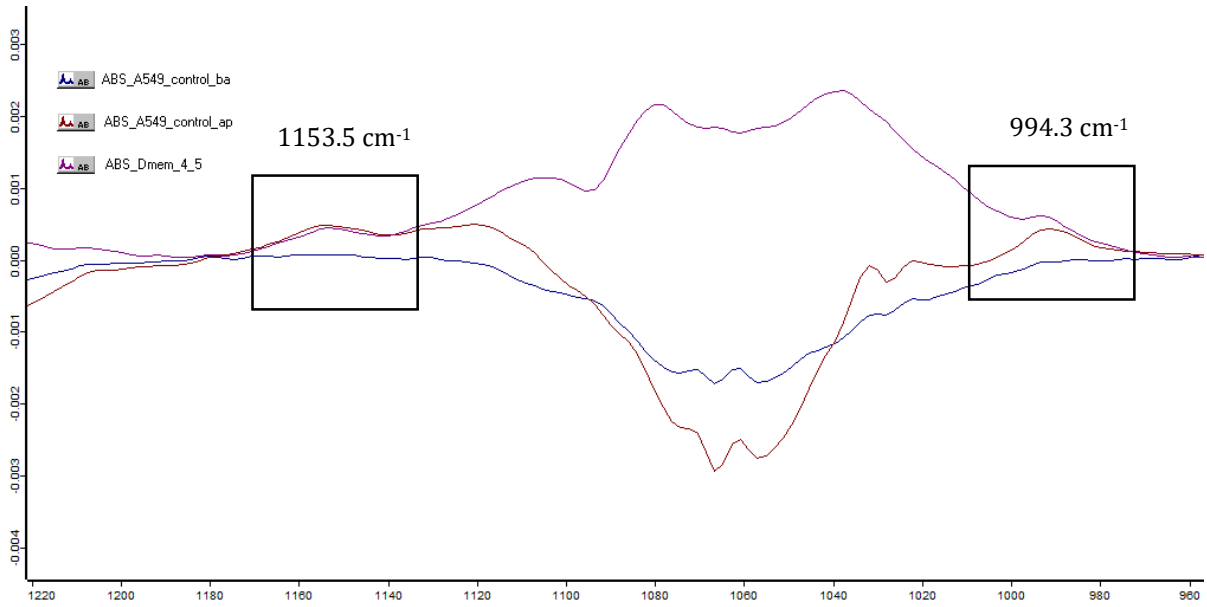

Figure 3.16: IR spectrum of negative interferences in basal and apical samples from transport inhibition experiments with 20 µM WZB-117 at day 8 post seeding. Violet spectrum displays the spectrum of high glucose DMEM for reference. The red and blue spectrum show IR absorbance data of the apical and basal sample. The spectrum at for the wavenumbers 1153.5 cm^{-1} and 994.3 cm^{-1} are highlighted.

Besides the A549 and BeWo b30 barrier, WZB-117 shows comparatively low inhibition strength in the barriers of Hep G2, HT-29 and Caco-2. The WZB-117 treated Hep G2 cells transfer 26.55% more glucose than PT treated cells, and 32.4% more glucose compared to CB treated cells. The transport differences are suggested to arise in the lower inhibition range of WZB-117, as it is a primary GLUT1 inhibitor.

The inhibition rates of the intestinal barriers behave similar to the inhibition rates of cytochalasin B. Compared to CB, HT-29 cells show a lower inhibition of 4% and Caco-2 cells 6% less. The inhibition in the co-culture of Caco-2 & HT-29 is slightly higher by 0.54% in comparison to CB. The results for Caco-2 and HT-29 reinforce the assumption that in the intestinal barriers the SGLT1 and GLUT2 distribution plays a major role in the glucose transfer.

Table 3.4: Evaluation table for glucose inhibition for all cell barriers after treatment with 20 µM CB, 30 µM PT or 20 µM WZB-117 for 24 hours. Glucose transport was measured after 60 minutes for CB and 120 minutes for PT and WZB-117 at day 8. Glucose concentration were analysed with IR spectroscopy at wavenumber 1035.7 cm^{-1} (* at wavenumber 1153.5 cm^{-1}). Inhibition is given in percentage to each cell control barrier without treatment.

Cell line/Co-culture	CB (60 min)	PT (120 min)	WZB-117 (120 min)
A549	35 ± 13%	20 ± 4.36%	8 ± 9%
BeWo b30	53 ± 11%	38 ± 12.16%	9 ± 8%
Caco-2	19± 8%	45 ± 16.24%	13 ± 8%
HT-29	12 ± 6%	25 ± 12%	8 ± 7%
Caco-2 & HT-29	16 ± 7%	27 ± 8%	16 ± 9%
Hep G2	42 ± 13%	36 ± 9%	10 ± 8%

4. Conclusion

In the current work a comparative evaluation of glucose transport processes in 5 human organ barriers was assessed. The barriers consisting of the lung, placenta, liver and intestines, were represented by human carcinoma cell lines in in-vitro. As the transport of glucose is accomplished by various passive and active glucose transporters, different inhibitors of the passive GLUT family and the active sodium-dependent SGLT family were discussed. Finally, their effects on glucose transfer and transporter on the carcinoma barriers were analysed and discussed.

Summarised, the inhibitor cytochalasin B showed the highest transport inhibitions in the placental BeWo b30 and hepatic Hep G2 barrier, in which both GLUT1 and GLUT3 are highly expressed. CB inhibition in the lung A549 cells exhibited a moderate inhibition of the expressed GLUT1, 3 4 and 12, although the amount of expression of these GLUTs is vaguely known. The intestinal barriers Caco-2 and HT-29 displayed an overall low inhibition with CB as GLUT2 and SGLT1 are not inhibited and supposedly responsible for the majority of glucose transport apart from GLUT1. In contrast, the glucose transport inhibitor phloretin differs from cytochalasin B in the ability to bind to the receptors of GLUT2 and SGLT1 [70, 76, 77]. It also has lower inhibitory strength for GLUT1 and GLUT4 compared to CB. However, it also shows affinities to the active transporter SGLT1. These differences lead to the primary inhibition of glucose in the intestinal cells, but lower inhibition in placental, hepatic and lung barriers. The results indicate that in placental and hepatic barrier the glucose transfer is mainly contributed by GLUT1 and GLUT3, and the glucose transfer in intestinal barriers by GLUT2 and SGLT1.

The GLUT1 inhibitor WZB-117 caused interferences in the infrared spectrum of lung and placental cells possibly due to cell death. However, the hepatic barrier developed significantly lower inhibition of glucose transfer for WZB-117 than other treated cells. The WZB-117 inhibition rates in the Caco-2 and HT-29 barriers are similar to the results of CB inhibition and reinforce the suggestion that GLUT2 and SGLT1 are essential transporters for glucose transfer in intestinal cells. However, the high anti-cancer effect of WZB-117 makes it questionable if the compound is suitable for transport inhibition experiments in cancer cell lines.

Furthermore, this work investigates the differences of glucose transporters between healthy human organs and cancer cell lines, which are used to represent them in-vitro. Many studies attempt to emulate more physiological organ barriers with dynamic organ-on-a chip technologies, as conventional in-vitro models show restrictions in simulating the physiological structures. In the work of Lee et al. [111], a placenta-on-a-chip was developed to investigate transport

characteristics of a microfluidic engineered placental barrier with the cancer cell line JEG-3, another choriocarcinoma cell line of the placenta. Models of a lung-on-a-chip were built to mimic situations in in-vivo with H1975 lung adenocarcinoma cells [112]. As these models try to increase the physiological significance of in-vitro studies, the principle question of the physiological relevance of the choice of cell model arise.

Future studies could investigate characteristics of glucose transport in primary cells, which are directly isolated from organ tissues. The comparison between primary cells and cancer cell lines could help to identify differences in transport characteristics or confirm the applicability of cancer cell lines as representation for human organ barriers.

5. References

1. Wood, I.S. and P. Trayhurn, *Glucose transporters (GLUT and SGLT): expanded families of sugar transport proteins.* Br J Nutr, 2003. **89**(1): p. 3-9.
2. Yihong Qiu, Y.C., Geoff G.Z. Zhang, Lirong Liu, William Porter, *Developing Solid Oral Dosage Forms: Pharmaceutical Theory and Practice*. 2009: Academic Press.
3. Encyclopedia.com. *Glucose*. [cited 2018 March 28]; The Columbia Encyclopedia, 6th ed:[Available from: http://www.encyclopedia.com/reference/encyclopedias-almanacs-transcripts-and-maps/glucose.
4. Offermanns, S., Rosenthal, Walter, *Encyclopedia of Molecular Pharmacology*. 2008: Springer.
5. Al-Haggar, M., *Fanconi-Bickel syndrome as an example of marked allelic heterogeneity.* World Journal of Nephrology, 2012. **1**(3): p. 63-68.
6. Burcelin, R., et al., *Liver hyperplasia and paradoxical regulation of glycogen metabolism and glucose-sensitive gene expression in GLUT2-null hepatocytes. Further evidence for the existence of a membrane-based glucose release pathway.* J Biol Chem, 2000. **275**(15): p. 10930-6.
7. Wang, D., et al., *Glut-1 deficiency syndrome: clinical, genetic, and therapeutic aspects.* Ann Neurol, 2005. **57**(1): p. 111-8.
8. Mergenthaler, P., et al., *Sugar for the brain: the role of glucose in physiological and pathological brain function.* Trends in neurosciences, 2013. **36**(10): p. 587-597.
9. Bell, A.W., W.W. Hay, Jr., and R.A. Ehrhardt, *Placental transport of nutrients and its implications for fetal growth.* J Reprod Fertil Suppl, 1999. **54**: p. 401-10.
10. Cetin, I. and G. Alvino, *Intrauterine growth restriction: implications for placental metabolism and transport. A review.* Placenta, 2009. **30 Suppl A**: p. S77-82.
11. Pedersen, J., *Weight and length at birth of infants of diabetic mothers.* Acta Endocrinol (Copenh), 1954. **16**(4): p. 330-42.
12. Garnett, J.P., E.H. Baker, and D.L. Baines, *Sweet talk: insights into the nature and importance of glucose transport in lung epithelium.* Eur Respir J, 2012. **40**(5): p. 1269-76.
13. Buhimschi, C.S. and C.P. Weiner, *Medications in pregnancy and lactation: part 1. Teratology.* Obstet Gynecol, 2009. **113**(1): p. 166-88.
14. Srinivasan, B., et al., *TEER measurement techniques for in vitro barrier model systems.* J Lab Autom, 2015. **20**(2): p. 107-26.
15. Groschwitz, K.R. and S.P. Hogan, *Intestinal Barrier Function: Molecular Regulation and Disease Pathogenesis.* The Journal of allergy and clinical immunology, 2009. **124**(1): p. 3-22.
16. BioNinja. *Types of Transport*. [cited 2018 21 March]; Available from: http://ib.bioninja.com.au/standard-level/topic-1-cell-biology/14-membrane-transport/types-of-transport.html.
17. Academy, K. *Passive transport and active transport across a cell membrane article*. [Article] October 20, 2014 [cited 2018 March 21]; Available from: https://www.khanacademy.org/test-prep/mcat/cells/transport-across-a-cell-membrane/a/passive-transport-and-active-transport-across-a-cell-membrane-article.
18. *The Cell Membrane*. [Article] 18/06/2004 [cited 2018 March 21]; Available from: http://www.biologymad.com/cells/cellmembrane.htm.

19. Academy, K. *Active transport*. [cited 2018 March 29]; Available from: https://www.khanacademy.org/science/biology/membranes-and-transport/active-transport/a/active-transport.
20. Team, P. *Secondary Active Transport*. 3 March 2014 [cited 2018 March 21]; Available from: http://www.physiologyweb.com/lecture_notes/membrane_transport/secondary_active_transport.html.
21. *The Glucosee Molecule - Chemical and Physical Properties*. [cited 2018 March 29]; Available from: https://www.worldofmolecules.com/foods/glucose.htm.
22. Barbara H. Stuart, D.J.A.E., *Biological Applications of Infrared Spectroscopy*. 1997.
23. By NEUROtiker - Own work, P.D. Wikipedia.
24. Thorens, B., *Facilitated glucose transporters in epithelial cells.* Annu Rev Physiol, 1993. **55**: p. 591-608.
25. Education, P. *Facilitated Diffusion and Active Transport of Glucose*. Concept 4-Review [cited 2018 March 21]; Available from: http://www.phschool.com/science/biology_place/biocoach/biomembrane1/glucose.html.
26. Tortora, G.J., *Principles of Anatomy and Physiology*. 2008: Wiley.
27. Mueckler, M. and B. Thorens, *The SLC2 (GLUT) Family of Membrane Transporters.* Molecular aspects of medicine, 2013. **34**(0): p. 121-138.
28. Harada, N. and N. Inagaki, *Role of sodium-glucose transporters in glucose uptake of the intestine and kidney.* Journal of Diabetes Investigation, 2012. **3**(4): p. 352-353.
29. Uldry, M., et al., *Identification of a mammalian H(+)-myo-inositol symporter expressed predominantly in the brain.* The EMBO Journal, 2001. **20**(16): p. 4467-4477.
30. Augustin, R., *The protein family of glucose transport facilitators: It's not only about glucose after all.* IUBMB Life, 2010. **62**(5): p. 315-33.
31. Zhao, F.Q. and A.F. Keating, *Functional properties and genomics of glucose transporters.* Curr Genomics, 2007. **8**(2): p. 113-28.
32. Kasahara, T. and M. Kasahara, *Expression of the rat GLUT1 glucose transporter in the yeast Saccharomyces cerevisiae.* Biochem J, 1996. **315 (Pt 1)**: p. 177-82.
33. Illsley, N.P., *Glucose transporters in the human placenta.* Placenta, 2000. **21**(1): p. 14-22.
34. Brown, K., et al., *Glucose transporter 3 (GLUT3) protein expression in human placenta across gestation.* Placenta, 2011. **32**(12): p. 1041-1049.
35. Hediger, M.A., et al., *Expression cloning and cDNA sequencing of the Na+/glucose co-transporter.* Nature, 1987. **330**(6146): p. 379-81.
36. Scheepers, A., H.G. Joost, and A. Schurmann, *The glucose transporter families SGLT and GLUT: molecular basis of normal and aberrant function.* JPEN J Parenter Enteral Nutr, 2004. **28**(5): p. 364-71.
37. Guillam, M.T., R. Burcelin, and B. Thorens, *Normal hepatic glucose production in the absence of GLUT2 reveals an alternative pathway for glucose release from hepatocytes.* Proc Natl Acad Sci U S A, 1998. **95**(21): p. 12317-21.
38. Matsui, C., et al., *Potential Roles of GLUT12 for Glucose Sensing and Cellular Migration in MCF-7 Human Breast Cancer Cells Under High Glucose Conditions.* Anticancer Res, 2017. **37**(12): p. 6715-6722.
39. Shah, S.W., et al., *Characterization of glucose transport and glucose transporters in the human choriocarcinoma cell line, BeWo.* Placenta, 1999. **20**(8): p. 651-9.

40. George Thompson, A.M., et al., *Inhibition of human GLUT1 and GLUT5 by plant carbohydrate products; insights into transport specificity.* Scientific Reports, 2015. **5**: p. 12804.
41. *solute carrier family 2 (SLC2, SLC2A)*. [cited 2018 March 31]; Available from: http://www.anvita.info/wiki/Solute_Carrier_Family_2.
42. Douard, V. and R.P. Ferraris, *Regulation of the fructose transporter GLUT5 in health and disease.* Am J Physiol Endocrinol Metab, 2008. **295**(2): p. E227-37.
43. Li, Q., et al., *Cloning and functional characterization of the human GLUT7 isoform SLC2A7 from the small intestine.* Am J Physiol Gastrointest Liver Physiol, 2004. **287**(1): p. G236-42.
44. Alam, F., et al., *Metabolic Control of Type 2 Diabetes by Targeting the GLUT4 Glucose Transporter: Intervention Approaches.* Curr Pharm Des, 2016. **22**(20): p. 3034-49.
45. Waller, A.P., et al., *GLUT12 functions as a basal and insulin-independent glucose transporter in the heart.* Biochim Biophys Acta, 2013. **1832**(1): p. 121-7.
46. medivizor.com, *Liver*.
47. http://www.lifeinharmony.me, *Anatomy Of Placenta Family GP*.
48. moziru.com, *Organs clipart lung - Pencil and in color organs clipart lung*.
49. bodytomy.com, *Large Intestine Anatomy*.
50. Sotak, M., J. Marks, and R.J. Unwin, *Putative tissue location and function of the SLC5 family member SGLT3.* Exp Physiol, 2017. **102**(1): p. 5-13.
51. Naifeh J, B.S., *Biochemistry, Carbohydrate, Aerobic Glycolysis.* Treasure Island (FL): StatPearls Publishing.
52. Otto Heinrich Warburg, F.D., *The metabolism of tumours*. 1930: London : Constable.
53. Zheng, J.I.E., Oncology Letters, 2012. **4**(6): p. 1151-1157.
54. Zu, X.L. and M. Guppy, *Cancer metabolism: facts, fantasy, and fiction.* Biochem Biophys Res Commun, 2004. **313**(3): p. 459-65.
55. Chung, F.-Y., et al., *GLUT1 gene is a potential hypoxic marker in colorectal cancer patients.* BMC Cancer, 2009. **9**(1): p. 241.
56. O'Byrne, K.J., et al., *Epigenetic Regulation of Glucose Transporters in Non-Small Cell Lung Cancer.* Cancers, 2011. **3**(2): p. 1550-1565.
57. Barron, C., E. Tsiani, and T. Tsakiridis, *Expression of the glucose transporters GLUT1, GLUT3, GLUT4 and GLUT12 in human cancer cells.* BMC Proceedings, 2012. **6**(Suppl 3): p. P4-P4.
58. Takanaga, H., B. Chaudhuri, and W.B. Frommer, *GLUT1 and GLUT9 as the major contributors to glucose influx in HEPG2 cells identified by a high sensitivity intramolecular FRET glucose sensor.* Biochimica et biophysica acta, 2008. **1778**(4): p. 1091-1099.
59. Gaither, K., A.N. Quraishi, and N.P. Illsley, *Diabetes alters the expression and activity of the human placental GLUT1 glucose transporter.* J Clin Endocrinol Metab, 1999. **84**(2): p. 695-701.
60. Illsley, N.P., M.C. Sellers, and R.L. Wright, *Glycaemic regulation of glucose transporter expression and activity in the human placenta.* Placenta, 1998. **19**(7): p. 517-524.
61. Bourgine, J., et al., *Gene expression profiling of systems involved in the metabolism and the disposition of xenobiotics: comparison between human intestinal biopsy samples and colon cell lines.* Drug Metab Dispos, 2012. **40**(4): p. 694-705.
62. Mahraoui, L., et al., *Expression and localization of GLUT-5 in Caco-2 cells, human small intestine, and colon.* Am J Physiol, 1992. **263**(3 Pt 1): p. G312-8.
63. Zheng, Y., et al., *Mechanisms of Glucose Uptake in Intestinal Cell Lines: Role of GLUT2.* Surgery, 2012. **151**(1): p. 13-25.

64. Hauptmann, S., et al., *Glucose transporter GLUT1 in colorectal adenocarcinoma cell lines is inversely correlated with tumour cell proliferation.* Anticancer Res, 2005. **25**(5): p. 3431-6.
65. Li, X., et al., *Downregulation of the Expression of GLUT1 Plays a Role in Apoptosis Induced by Sodium Butyrate in HT-29 Cell Line.* International Journal of Molecular Sciences, 2006. **7**(2).
66. Steffansen, B., et al., *SGLT1-Mediated Transport in Caco-2 Cells Is Highly Dependent on Cell Bank Origin.* J Pharm Sci, 2017. **106**(9): p. 2664-2670.
67. Paola De Luca, F.A., Margherita Maggioni, Elena Donetti, Amelia Fiorilli, Anita Ferraretto, *Morphology related functionality in Caco2/HT-29 co-culture cells: a versatile model of human intestinal epithelium.* ITALIAN JOURNAL OF ANATOMY AND EMBRYOLOGY.
68. Ojelabi, O., et al., *WZB117 (2-Fluoro-6-(m-hydroxybenzoyloxy) Phenyl m-Hydroxybenzoate) Inhibits GLUT1-mediated Sugar Transport by Binding Reversibly at the Exofacial Sugar Binding Site*. 2016.
69. Carruthers, A., et al., *Will the original glucose transporter isoform please stand up!* Am J Physiol Endocrinol Metab, 2009. **297**(4): p. E836-48.
70. Hellwig, B. and H.G. Joost, *Differentiation of erythrocyte-(GLUT1), liver-(GLUT2), and adipocyte-type (GLUT4) glucose transporters by binding of the inhibitory ligands cytochalasin B, forskolin, dipyridamole, and isobutylmethylxanthine.* Mol Pharmacol, 1991. **40**(3): p. 383-9.
71. Wu, C.H., et al., *In vitro and in vivo study of phloretin-induced apoptosis in human liver cancer cells involving inhibition of type II glucose transporter.* Int J Cancer, 2009. **124**(9): p. 2210-9.
72. Carruthers, A. and A.L. Helgerson, *Inhibitions of sugar transport produced by ligands binding at opposite sides of the membrane. Evidence for simultaneous occupation of the carrier by maltose and cytochalasin B.* Biochemistry, 1991. **30**(16): p. 3907-3915.
73. Nelson, J.A. and R.E. Falk, *Phloridzin and phloretin inhibition of 2-deoxy-D-glucose uptake by tumor cells in vitro and in vivo.* Anticancer Res, 1993. **13**(6a): p. 2293-9.
74. Kasahara, T. and M. Kasahara, *Characterization of rat Glut4 glucose transporter expressed in the yeast Saccharomyces cerevisiae: comparison with Glut1 glucose transporter.* Biochim Biophys Acta, 1997. **1324**(1): p. 111-9.
75. Dawson, P.A., et al., *Sequence and functional analysis of GLUT10: a glucose transporter in the Type 2 diabetes-linked region of chromosome 20q12-13.1.* Mol Genet Metab, 2001. **74**(1-2): p. 186-99.
76. Raja, M., et al., *Chapter Two - SLC5 and SLC2 Transporters in Epithelia—Cellular Role and Molecular Mechanisms*, in *Current Topics in Membranes*, M.O. Bevensee, Editor. 2012, Academic Press. p. 29-76.
77. Hirayama, B.A., A. Díez-Sampedro, and E.M. Wright, *Common mechanisms of inhibition for the Na(+)/glucose (hSGLT1) and Na(+)/Cl(−)/GABA (hGAT1) cotransporters.* British Journal of Pharmacology, 2001. **134**(3): p. 484-495.
78. Pajor, A.M., et al., *Inhibitor binding in the human renal low- and high-affinity Na+/glucose cotransporters.* J Pharmacol Exp Ther, 2008. **324**(3): p. 985-91.
79. Bianchi, L. and A. Díez-Sampedro, *A Single Amino Acid Change Converts the Sugar Sensor SGLT3 into a Sugar Transporter.* PLoS ONE, 2010. **5**(4): p. e10241.
80. Song, P., et al., *Sodium glucose cotransporter SGLT1 as a therapeutic target in diabetes mellitus.* Expert opinion on therapeutic targets, 2016. **20**(9): p. 1109-1125.

81. Kwon, O., et al., *Inhibition of the intestinal glucose transporter GLUT2 by flavonoids.* Faseb j, 2007. **21**(2): p. 366-77.
82. Kellett, G.L. and P.A. Helliwell, *The diffusive component of intestinal glucose absorption is mediated by the glucose-induced recruitment of GLUT2 to the brush-border membrane.* Biochemical Journal, 2000. **350**(Pt 1): p. 155-162.
83. Kellett, G.L. and E. Brot-Laroche, *Apical GLUT2: a major pathway of intestinal sugar absorption.* Diabetes, 2005. **54**(10): p. 3056-62.
84. Nybacka, L., *FTIR spectroscopy of glucose*, in *Department of Engineering Sciences, Solid State Electronics*. 2016, Uppsala University, Disciplinary Domain of Science and Technology.
85. Kasahara, R., et al., *Noninvasive glucose monitoring using mid-infrared absorption spectroscopy based on a few wavenumbers.* Biomedical Optics Express, 2018. **9**(1): p. 289-302.
86. G. Osborne, B., *Near-Infrared Spectroscopy in Food Analysis*. 2006.
87. Heise, H.M., *Glucose Measurements by Vibrational Spectroscopy.* Handbook of Vibrational Spectroscopy by John Wiley & Sons, Ltd, 2006.
88. Witkowska Nery, E., et al., *Electrochemical Glucose Sensing: Is There Still Room for Improvement?* Analytical Chemistry, 2016. **88**(23): p. 11271-11282.
89. Nielsen, S.S., *Food Analysis*. 2017: Springer.
90. Helmut Günzler, H.M.H., *IR-Spektroskopie: Eine Einführung*. 3 ed. 1996: Wiley-VCH. 397
91. Wei, Q., *Surface Modification of Textiles*. 2009: Elsevier.
92. Spencer L. Seager, M.R.S., Maren S. Hansen, *Chemistry for Today: General, Organic, and Biochemistry, 9th Edition*.
93. Medhat Ahmed Ibrahim, M.A., Hanan El-Haes, Abraham F. Jalbout, Aned de Leon, *Analysis of the structure and vibrational spectra of glucose and fructose.* Eclética Química Journal, 2006.
94. WORLD PRECISION INSTRUMENTS, I., *EVOM2 Epithelial Voltohmmeter*. 2016.
95. Alankar Shrivastava, V.B.G., *Methods for the determination of limit of detection and limit of quantitation of the analytical methods.* Chronicles of Young Scientists, 2011. **2**(1): p. 21-25.
96. Blume, L.F., et al., *Temperature corrected transepithelial electrical resistance (TEER) measurement to quantify rapid changes in paracellular permeability.* Pharmazie, 2010. **65**(1): p. 19-24.
97. Hollinger, J.O., *An Introduction to Biomaterials, Second Edition*. 2 ed. 2011: CRC Press.
98. Engle, M.J., G.S. Goetz, and D.H. Alpers, *Caco-2 cells express a combination of colonocyte and enterocyte phenotypes.* J Cell Physiol, 1998. **174**(3): p. 362-9.
99. Heaton, S.J., et al., *The use of BeWo cells as an in vitro model for placental iron transport.* Am J Physiol Cell Physiol, 2008. **295**(5): p. C1445-53.
100. Martínez-Maqueda, D., B. Miralles, and I. Recio, *HT29 Cell Line*, in *The Impact of Food Bioactives on Health: in vitro and ex vivo models*, K. Verhoeckx, et al., Editors. 2015, Springer International Publishing: Cham. p. 113-124.
101. Briske-Anderson, M.J., J.W. Finley, and S.M. Newman, *The influence of culture time and passage number on the morphological and physiological development of Caco-2 cells.* Proc Soc Exp Biol Med, 1997. **214**(3): p. 248-57.
102. Cooper, J.R., et al., *Long Term Culture of the A549 Cancer Cell Line Promotes Multilamellar Body Formation and Differentiation towards an Alveolar Type II Pneumocyte Phenotype.* PLoS One, 2016. **11**(10): p. e0164438.

103. Aengenheister, L., et al., *An advanced human in vitro co-culture model for translocation studies across the placental barrier.* Scientific Reports, 2018. **8**(1): p. 5388.
104. Sule-Suso, J., et al., *Effects of CaCl2 and MgCl2 on Fourier transform infrared spectra of lung cancer cells.* Appl Spectrosc, 2004. **58**(1): p. 61-7.
105. Chen, L., B. Tuo, and H. Dong, *Regulation of Intestinal Glucose Absorption by Ion Channels and Transporters.* Nutrients, 2016. **8**(1): p. 43.
106. Jansson, T., M. Wennergren, and N.P. Illsley, *Glucose transporter protein expression in human placenta throughout gestation and in intrauterine growth retardation.* J Clin Endocrinol Metab, 1993. **77**(6): p. 1554-62.
107. Gaudenzi, S., et al., *Cell apoptosis specific marker found by Fourier Transform Infrared Spectroscopy.* Spectroscopy, 2004. **18**: p. 415-422.
108. Papaliagkas, V., et al., *The proteins and the mechanisms of apoptosis: A mini-review of the fundamentals.* Hippokratia, 2007. **11**(3): p. 108-113.
109. Min, J.I.E., et al., *Phloretin induces apoptosis of non-small cell lung carcinoma A549 cells via JNK1/2 and p38 MAPK pathways.* Oncology Reports, 2015. **34**(6): p. 2871-2879.
110. Liu, Y., et al., *A small-molecule inhibitor of glucose transporter 1 downregulates glycolysis, induces cell-cycle arrest, and inhibits cancer cell growth in vitro and in vivo.* Mol Cancer Ther, 2012. **11**(8): p. 1672-82.
111. Lee, J.S., et al., *Placenta-on-a-Chip: A novel platform to study the biology of the human placenta.* The journal of maternal-fetal & neonatal medicine : the official journal of the European Association of Perinatal Medicine, the Federation of Asia and Oceania Perinatal Societies, the International Society of Perinatal Obstetricians, 2016. **29**(7): p. 1046-1054.
112. Hassell, B.A., et al., *Human Organ Chip Models Recapitulate Orthotopic Lung Cancer Growth, Therapeutic Responses, and Tumor Dormancy In Vitro.* Cell Rep, 2017. **21**(2): p. 508-516.